Journal of Inorganic Biochemistry 190 (2019) 45–66

Contents lists available at ScienceDirect

Journal of Inorganic Biochemistry

journal homepage: www.elsevier.com/locate/jinorgbio

A novel binuclear hydrazone-based Cd(II) complex is a strong pro-apoptotic inducer with significant activity against 2D and 3D pancreatic cancer stem cells

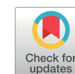

Snežana Bjelogrlić[a,b], Tamara R. Todorović[c], Ilija Cvijetić[d], Marko V. Rodić[e], Miroslava Vujčić[f], Sanja Marković[c], Jovana Araškov[c], Barbara Janović[f], Fathi Emhemmed[b], Christian D. Muller[b], Nenad R. Filipović[g,*]

[a] National Cancer Research Center of Serbia, Pasterova 14, Belgrade, Serbia
[b] Institut Pluridisciplinaire Hubert Curien, UMR 7178 CNRS Université de Strasbourg, 67401 Illkirch, France
[c] Faculty of Chemistry, University of Belgrade, Studentski trg 12-16, Belgrade, Serbia
[d] Innovation Center of the Faculty of Chemistry, University of Belgrade, Studentski trg 12-16, Belgrade, Serbia
[e] Faculty of Sciences, University of Novi Sad, Trg Dositeja Obradovića 3, Novi Sad, Serbia
[f] Institute of Chemistry, Technology and Metallurgy, University of Belgrade, Njegoševa 12, Belgrade, Serbia
[g] Faculty of Agriculture, University of Belgrade, Nemanjina 6, Belgrade, Serbia

ARTICLE INFO

Keywords:
Cd(II) complex
Hydrazones
Apoptosis
Cancer stem cells
DNA interactions
HSA interactions

ABSTRACT

A novel binuclear Cd complex (**1**) with hydrazone-based ligand was prepared and characterized by spectroscopy and single crystal X-ray diffraction techniques. Complex **1** reveals a strong pro-apoptotic activity in both human, mammary adenocarcinoma cells (MCF-7) and pancreatic AsPC-1 cancer stem cells (CSCs). While apoptosis undergoes mostly caspase-independent, **1** stimulates the activation of intrinsic pathway with noteworthy down regulation of caspase-8 activity in respect to non-treated controls. Distribution of cells over mitotic division indicates that **1** caused DNA damage in both cell lines, which is confirmed in DNA interaction studies. Compared to **1**, cisplatin (CDDP) does not achieve cell death in 2D cultured AsPC-1 cells, while induces different pattern of cell cycle changes and caspase activation in 2D cultured MCF-7 cells, implying that these two compounds do not share similar mechanism of action. Additionally, **1** acts as a powerful inducer of mitochondrial superoxide production with dissipated trans-membrane potential in the majority of the treated cells already after 6 h of incubation. On 3D tumors, **1** displays a superior activity against CSC model, and at 100 μM induces disintegration of spheroids within 2 days of incubation. Fluorescence spectroscopy, along with molecular docking show that compound **1** binds to the minor groove of DNA. Compound **1** binds to the human serum albumin (HSA) showing that the HSA can effectively transport and store **1** in the human body. Thus, our current study strongly supports further investigations on antitumor activity of **1** as a drug candidate for the treatment of highly resistant pancreatic cancer.

1. Introduction

Cellular malignancy has continually been one of leading cause of death worldwide. The main relying reason of fatal outcome in malignant patients is the development of multidrug resistance and disease relapse [1]. Most cancer cells proliferate more rapidly than their normal counterparts; therefore, most cancer drugs target the cell cycle, either directly by inhibition of the mitotic spindle, preventing equal division of DNA to the two daughter cells, or indirectly *via* DNA damaging [2]. Cisplatin (*cis*-[$PtCl_2(NH_3)_2$]; CDDP) is the first metal-based chemoterapeutic approved by The Food and Drug Administration agency in 1978, for which DNA was established as molecular target [3]. Because of its effectiveness in treating a variety of cancers, especially testicular cancer, for which it has a > 90% cure rate [4], it become a blockbuster drugs since it remains among the most widely used anticancer chemotherapeutics and component in more active clinical trials than any other anticancer agent [5]. There were investigations of biological activity of metal-based compounds before the discovery of anticancer properties of CDDP in 1969 [6]. Nevertheless, its tremendous success as well as research which started in order to study its

* Corresponding author at: Faculty of Agriculture, University of Belgrade, Nemanjina 6, Belgrade, Serbia.
E-mail address: nenadf@agrif.bg.ac.rs (N.R. Filipović).

https://doi.org/10.1016/j.jinorgbio.2018.10.002
Received 15 June 2018; Received in revised form 16 September 2018; Accepted 3 October 2018
Available online 14 October 2018
0162-0134/ © 2018 Elsevier Inc. All rights reserved.

mechanism of action and improve its side effects by developing new metal complexes based on platinum and other metals, was the landmark and beginning of modern era of Medicinal Inorganic Chemistry [7]. As a result of such efforts another six CDDP analogues have been registered as anticancer drugs up to now worldwide [8]. The common characteristic of all platinum-based approved chemoterapeutics is covalent binding to DNA, preferably to guanine, resulting in intrastrand and interstrand DNA cross-links [5,9].

Nowadays almost 50% of reports on biological activity of metal-containing compounds involve evaluation of their DNA interaction properties. Although, DNA is generally accepted as a major pharmacological target of the majority of metal-based drugs, there are certain gaps in this paradigm [10]. On the other hand, there are huge number of evidences that proteins also represent significant cellular targets for metal complexes [11–14].

A scarcely explored part of medicinal inorganic chemistry is that related to the potential anticancer activity of Cd complexes, since it has been classified by the International Agency for Research on Cancer as a human carcinogen [15]. Cadmium toxicity derives from the fact that it is rapidly localized intracellularly, mainly in the liver, and then is bound to metallothionein forming a complex that is slowly transferred to the bloodstream to be deposited in the kidneys [16]. Some studies indicate that Cd may exert a paradoxical effect in cancer perhaps dependent on the form it exists in: free Cd, protein-bound Cd, and Cd complexes. It seems that ligand type used for preparation of Cd complexes may cause their very favorable anti-tumor effects [17]. Ligands used for preparation of Cd complexes can be classified as: thiosemicarbazones [16,18–24], selenosemicarbazones [25–27], hydrazones [16,27–36], hydrazides [38,39], diimines [40], amides [41,42], aminoacids [43,44], heterocycles [44–56], macrocycles [58–60], drugs [61–64], scorpionates [65], natural products [66], thiocarbazates [67–71] and piperazines [72]. Antiproliferative screening results revealed that in many cases complexation with Cd resulted in better activity of obtained complexes in comparison to free ligands [15,20–22, 34–37,39,43–47,59–63,66–68,71] and approved chemotherapeutics [15,19–22,28,31,36,37,39,40,57,60–63,66–69]. Comparative studies with Zn(II), Cu(II), Co(II), Ni(II), Ce(IV), Zr(IV), Mn(II), Pb(II), Ca(II), and Sn(II) metal complexes revealed that Cd(II) complexes possess better activities [17,21,23,34,36,41,47,49,53,57,61,71]. Mechanistic studies revealed that Cd(II) complexes kill cancer cells *via* apoptosis [25,34,35,38,41,43,54,56,59,71]. Some of the investigated complexes target DNA non-covalently by groove binding [20], intercalation [36,38,54,57,60,64] and combined mode of intercalation and groove binding [45], while in some cases nuclease activity [31,54,57] and covalent binding similar to CDDP were observed [30]. Also, proteasomal chymotrypsin-like [34,35,44], proteasomal deubiquitinase [56], histone deacetylase [43] and telomerase [72] inhibiton properties were revealed as mode of action of several Cd complexes, as well as inhibition of incorporation of 3H-thymidine into DNA and the respiration of tumor cells [18].

In our previous work we investigated biological activity of metal complexes with hydrazone-based ligands obtained from ethyl hydrazinoacetate hydrochloride (haOEt × HCl) and variuous *N*-heteroaromatic carbonyl compounds [73–79]. Among the investigated compounds with this type of ligands Zn, Cu and Pd complexes showed promising anticancer activities [77–79], while Cd compounds have not been investigated yet. In the current investigation, we prepared a novel Cd complex by reaction of haOEt × HCl and *N*-heteroaromatic carbonyl compound 2-acetylpyridine (2-ap) and tested its anticancer activity on two distinctive cell lines. Human mammary adenocarcinoma cells (MCF-7) are well known and widely used model for investigation of drug activity against breast cancer. Instead of being a cloned cell line where all cells share identical features, MCF-7 cell culture is a population of diverse phenotypes due to different gene expression profile of cells [80]. Particular characteristic arises from previously defined ability of breast cancer cells to reproduce phenotypic equilibrium of the initial tumor bulk when are cultured *in vitro* conditions [81]. Another cell line used in this study represents cancer stem cell (CSC) model of pancreatic adenocarcinoma (AsPC-1), highly resistant to majority of chemotherapeutic agents used nowadays [82,83] Within a tumor bulk, CSCs consist scarce subpopulation of immortal cells that are dividing rapidly unlike stem cells of healthy tissues [84]. CSCs are endowed with significantly enhanced DNA repairing mechanisms, which together with their extensive genomic heterogeneity result in creation of multifarious sub-clones. Each sub-clone has unique epigenomic profile that enables development of resistant phenotypes to applied anticancer treatments [85]. Furthermore, CSCs can resort in the dormancy phase, which is unique strategy to avoid harmful effects of chemotherapeutical and radiation treatments that target rapidly dividing cells [86,87]. Thus, therapy-induced dormancy is tactical response of CSCs to acquire epigenetic alterations that are necessary for adaptation to new microenvironment afterwards they relapse as a more aggressive, drug-resistant phenotype [88]. Treatment that would successfully eliminate CSCs should either trigger their apoptotic death, or to interfere with their ability to refuge in dormancy by means of induced differentiation, therefore increasing their vulnerability to chemo- and radio-therapy. Up to date, there is no still efficient treatment option against CSCs. Establishment of new treatment strategy that would efficiently eliminate CSCs is set as a crucial need in the cure of malignancy. For those reasons, our study has been arranged to assess competency of **1** to cause cell death in CSCs and non-CSCs and estimate its ability to act as comprehensive anticancer agent that could provide eradication of malignant disease. Here, we investigated activity of **1** on standardly used two-dimensional (2D) monolayer cell culture and on three-dimensional (3D) spheroidal model. The latter, closer to CSCs in a metastatic environment, is a well-established screening platform known to provide more reliable readouts on drug activity as compared to classical 2D framework [89].

2. Experimental

2.1. Chemicals and instrumentation

2-Acetylpyridine (99 + %) was obtained from Acros Organics, while ethyl hydrazinoacetate hydrochloride (97%) and $Cd(AcO)_2 \times 2H_2O$ (p.a.) were obtained from Fluka. All solvents (methanol 99%, diethyl ether 98.0%) were used without further purification. Elemental analyses (C, H, N) were performed by the standard micro-methods using an ELEMENTARVario ELIII C.H.N.S. = O analyzer. IR spectrum was recorded on a Thermo Scientific Nicolet 6700 FT-IR spectrophotometer by the Attenuated Total Reflection (ATR) technique in the region 4000–400 cm^{-1} (Fig. S1, Supplementary material). Abbreviations used for IR spectrum: vs, very strong; s, strong; m, medium; w, weak. Molar conductivity was measured at room temperature (25 °C) on a digital multimeter CRISON MM41. All NMR spectral measurements were performed on a Bruker Avance III 500 spectrometer equipped with a broad-band direct probe. The spectra were recorded at room temperature in DMSO-d_6. Chemical shifts are given on δ scale relative to tetramethylsilane as internal standard for ^{1}H and ^{13}C or $Cd(ClO_4)_2$ in D_2O as external standard for ^{113}Cd. Coupling constants (*J*) were expressed in Hz. Abbreviations used for NMR spectra: s, singlet; d, doublet; t, triplet; br. broad. 1D and 2D spectra are shown in Figs. S2–S11 (Supplementary material). UV–visible (UV–Vis) spectra were recorded on a GBC Scientific Cintra 6 UV–Vis spectrophotometer (200–1000 nm), using sample dissolved in DMSO (Fig. S12, Supplementary material).

2.2. Synthesis of $[Cd_2Cl_2(AcO)_2(aphaOMe)_2]$ (1)

A solution of haOEt × HCl (0.18 g, 1.16 mmol) and 2-ap (0.14 g, 1.16 mmol) in 20 mL of MeOH was stirred at 40 °C and then solid Cd $(AcO)_2 \times 2H_2O$ (0.31 g, 1.16 mmol) was added in the reaction mixture. The resulting solution was stirred for 30 min at 40 °C. White crystals

were obtained after slow evaporation of the solvent at the room temperature after three days. The crystals were filtered off and washed with cold ethanol and diethyl ether. Yield: 0.28 g (58%). Anal. Calcd. for $C_{24}H_{32}Cl_2Cd_2N_6O_8$ (%): C, 34.80; H, 3.89; N, 10.15. Found: C, 34.66; H, 3.81, N, 10.12. Λ_M (2.17×10^{-3} M, H_2O) = 20.0 Ω^{-1} cm^2 mol^{-1}. IR (ATR, ν_{max}/cm^{-1}): 3263 (m), 1752 (s), 1597 (m), 1541 (vs), 1478 (vs), 1199 (vs), 1016 (m), 642(w), 459 (w). ^{1}H NMR (500.26 MHz, DMSO-d_6) δ: 1.80 (s, 3H), 2.22 (s, 3H), 3.61 (s, 3H), 4.25 (d, 1H, ^3J = 5.5 Hz), 7.23 (br. t, 1H, ^3J = 5.5 Hz), 7.42 (t, 1H), 7.84 (d, 1H, ^3J = 8.5 Hz), 7.91 (br. t, 1H, ^3J = 8.5 Hz), 8.62 (br. d, 1H). ^{13}C NMR (126.0 MHz, DMSO-d_6) δ: 11.7, 21.8, 51.0, 51.2, 120.9, 123.6, 138.8, 140.7, 148.9, 152.4, 171.6, 177.2. ^{113}Cd NMR (110.95 MHz, DMSO-d_6) δ: 139.3.

2.3. Crystal structure determination

Diffraction data were collected on a Gemini S diffractometer (Oxford Diffraction), equipped with a Mo $K\alpha$ radiation source (λ = 0.71073 Å) and a Sapphire CCD detector. Data collection strategy calculation and data reduction were performed with the *CrysAlisPro* [90]. Structure was solved by *SHELXT* [91], and refined with the *SHELXL*-2014 [92]. The *SHELXLE* [93] was used as a graphical user interface for the refinement procedures. All non-hydrogen atoms were refined anisotropically. The hydrogen atoms attached to C atoms were placed at geometrically idealized positions with C-H distances fixed to 0.93 and 0.96 Å for sp^2 and sp^3 C atoms, respectively. Their isotropic displacement parameters were set equal to 1.2 and 1.5 U_{eq} of the parent sp^2 and sp^3 C atoms, respectively. The hydrogen atoms attached to N atoms were located in difference Fourier map and refined isotopically. Structures were validated with *PLATON* [94] together with extensive use of *Mercury CSD* 2017 [95] and Cambridge Crystallographic Database (CSD) [96].

A summary of the crystallographic data for crystal structure is given in Table 1. CCDC 1831819 contains the Supplementary crystallographic data for this paper. These data can be obtained free of charge from The Cambridge Crystallographic Data Centre via https://www.ccdc.cam.ac.uk/structures/.

Calculation of intermolecular interaction energies were performed by using CE-HF model energies [97] embodied in *CrystalExplorer17* [98]. Prior to calculations, the lengths of X–H bonds were normalized to standard neutron diffraction values. A Hirshfeld surface [99] was calculated for a molecule in the crystal structure, and the number of surface patches was determined to be 18, thus defining the coordination number of a molecule. Calculations were performed for all 18 molecular pairs comprising of the central molecule and one neighboring molecule.

Table 1
Crystallographic and refinement details for **1**.

Chemical formula	$C_{24}H_{32}Cd_2Cl_2N_6O_8$
M_r	828.25
Crystal system	Monoclinic
Space group	$P2_1/n$
Temperature (K)	294
a (Å)	8.9762 (5)
b(Å)	13.1627 (7)
c (Å)	13.7226 (8)
β (°)	97.488 (5)
V (Å^3)	1607.51 (16)
Z	2
Radiation type	Mo $K\alpha$
μ (mm^{-1})	1.54
Crystal size (mm)	0.35 × 0.13 × 0.09
Absorption correction	Analytical
T_{min}, T_{max}	0.671, 0.877
Measured reflections	14,721
Independent reflections	3898
Observed reflections [$I > 2\sigma(I)$]	2714
R_{int}	0.044
(sin $\theta/\lambda)_{max}$ (Å^{-1})	0.683
$R[F^2 > 2\sigma(F^2)]$	0.048
$wR(F^2)$	0.131
S	1.07
No. of parameters	196
No. of restraints	1
H-atom treatment	Mixed
$\Delta\rho_{max}$, $\Delta\rho_{min}$ (e Å^{-3})	0.72, −0.93

2.4. Evaluation of biological activity and computational studies

Detailed protocols for anticancer related experiments (Annexin V and propidium iodide staining, calculation of ApoC$_{50}$ concentration, cell cycle analysis, inhibition of caspase activity, evaluation of caspase-8 and -9 activities, determination of mitochondrial superoxide generation, assessment of changes in mitochondrial potential and growth inhibition of 3D tumor models), DNA binding experiments (agarose gel electrophoresis and fluorescence measurements), human serum albumin (HSA) interaction experiments, acute lethality assay, as well as details regarding computational studies can be found in Supplementary material.

3. Results and discussion

3.1. Synthesis and characterization of 1

In our previous work complexes with ligands based on haOEt × HCl and *N*-heteroaromatic carbonyl compounds were obtained by template reactions involving corresponding metal salts [73–79,100,101]. It was found that reactive ethyl-ester group can undergo hydrolysis [100,101] or trans-esterification reaction and that this processes can be directed by the solvent used for metal complex preparation [79]. Previously, we have obtained the Cd(II) complexes with aphaOEt ligand (Scheme 1A), which represents a condensation product of haOEt × HCl and 2-ap, by using EtOH as a solvent [76,100]. In this work a novel Cd(II) complex with methyl-ester analogue of aphaOEt, *i.e.* aphaOMe ligand (Scheme 1A), was prepared by template reaction of $Cd(AcO)_2 \times 2H_2O$, 2-ap and haOEt × HCl in MeOH (Scheme 1B).

The results of elemental analysis confirmed that aphaOMe ligand was formed and that there is one chloride, one acetate and one cadmium ion per ligand molecule. The existence of acetate anion in **1** was confirmed by IR spectroscopy. Two very strong bands, characteristic for bidentate acetate coordination, were observed at 1541 (ν_{as}) and 1478 (ν_s) cm^{-1} [102]. The molar conductivity of **1** in water is 20.0 Ω^{-1} cm^2 mol^{-1}, which is significantly less than threshold value for 1:1 electrolytes [103], confirming that **1** is molecular coordination compound. The general formula of **1** [$Cd_2Cl_2(AcO)_2(aphaOMe)_2$], is unequivocally derived from a single crystal X-ray diffraction experiment (*vide infra*).

3.2. Description of crystal structure

ORTEP drawings of the asymmetric unit and molecular structure of binuclear complex **1** are depicted in Fig. 1. The complex lies at the centre of inversion at 1 ½ ½. Each cadmium ion is coordinated with pyridine and imine nitrogen atoms from *in situ* obtained aphaOMe ligand, two oxygen atoms from acetate ion and two bridging chloride ions [Cl(1) and its symmetry equivalent at 2 − *x*, 1 − *y*, 1 − *z*]. Due to deviation of ligands' and acetate ion bite angles from an ideal value of 90°, the geometry around each cadmium ion is distorted octahedral. The *cis* bond angles are in the wide range from 54.8 to 116.9°, while the *trans* ones vary from 142.0 to 160.1° (Table 2). All coordinative bond lengths are in the usual range (Table 2). As previously noted for related Cu(II) and Cd(II) complexes [74,76], the ester oxygen atom from aphaOMe ligand is not involved in coordination.

3D crystal packing is based on hydrogen bonds and π-π stacking interactions. Each NH group of the ligand is involved in hydrogen bonding

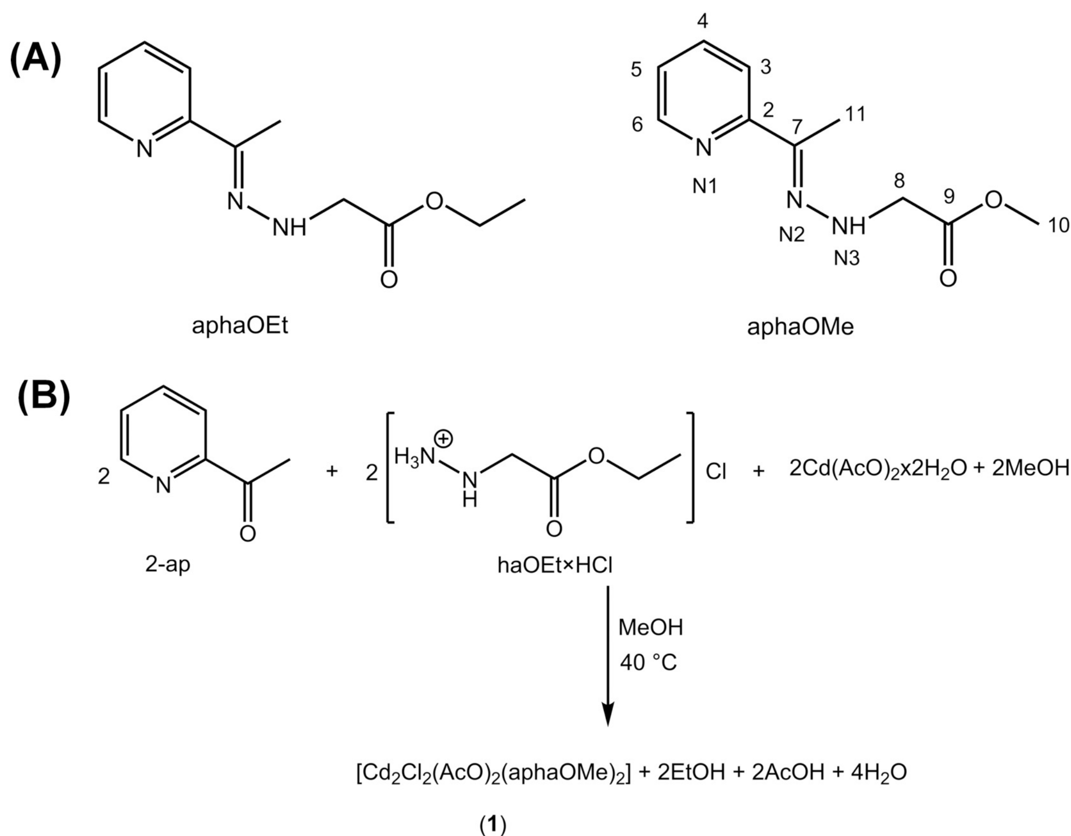

Scheme 1. (A) Structures of aphaOEt and aphaOMe ligands. (B) Synthesis of **1**.

with one of the acetate oxygen atoms of another complex molecule (N3⋯O3^i = 2.889(7) Å, N3—H3A⋯O3^i = 149(4)°, $i = {}^3/_2 - x, -½ + y, ½ - z$) with formation of 2D layers parallel to (1 0 −1) (Fig. 2A). Pyridine fragments are involved in π-π interactions with centroid-centroid distance of 3.675(4) Å. Stacked rings are almost perfectly align with face-to-face orientation, as indicated by the corresponding displacement angle of 13.5° and respective shift of 0.861 Å [104]. The stacking interactions between neighboring complex molecules expand binuclear units into 1D supramolecular chains running along [100] direction (Fig. 2B). Within these chains, two out of four aromatic protons are involved in weak hydrogen bonds with one of the acetate oxygen atoms and chloride bridges from neighboring complex units (C4⋯O4^i = 3.305(8) Å, C4—H4⋯O4^i = 158°, $i = -1 + x, y, z$; C3⋯Cl1^{ii} = 3.546(8) Å, C3—H3⋯Cl1^{ii} = 145°, $ii = 1 - x, 1 - y, 1 - z$) (Fig. 2B).

To better understand crystal packing determinants, a qualitative ranking of intermolecular interactions is necessary, as qualitative reasoning on intermolecular cohesion, based only on geometrical parameters, can sometimes lead to erroneous conclusions [105]. Therefore, a calculation of pairwise intermolecular interaction energies by whole-of-molecule approach, which avoids the focus on specific atom–atom interactions, was performed. The resulting interaction energies are summarized in Table S1 (Supplementary material). A general conclusion is that both electrostatic and dispersion terms play equally important role in total interaction energies. The largest stabilizing energy (−158 kJ mol^{-1} per pair) is associated with two pairs comprising 1D supramolecular chains running along [100] direction, while the interaction energy between four molecular pairs involved in formation of 2D

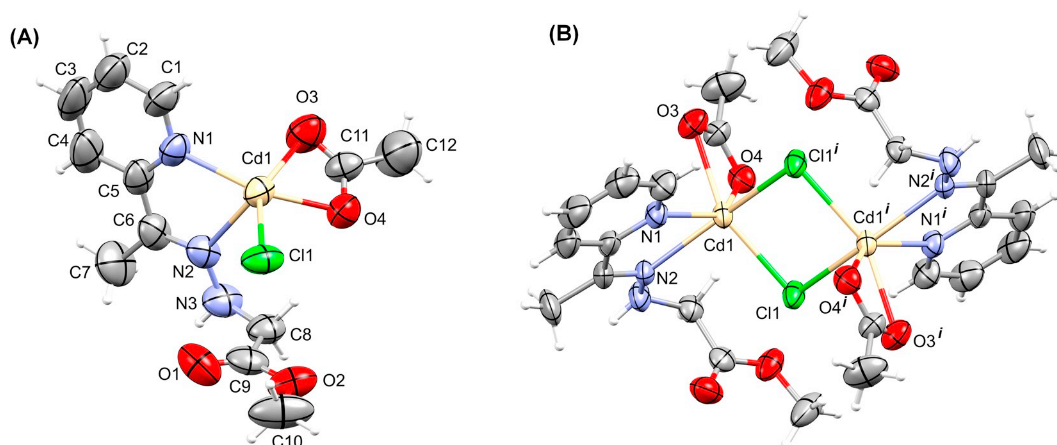

Fig. 1. Asymmetric unit (A) and perspective view and labelling of the molecular structure of **1** (B). Thermal ellipsoids are at the 40% probability level. Equivalent atoms are generated by the transformation $i = 2 - x, 1 - y, 1 - z$.

Table 2
Selected bond lengths (Å) and angles (°) for **1**, with esd's in parentheses.

Cd(1)–N(1)	2.281(4)
Cd(1)–N(2)	2.399(4)
Cd(1)–O(3)	2.416(4)
Cd(1)–O(4)	2.273(4)
Cd(1)–Cl(1)	2.5457(13)
Cd(1)–Cl(1)^{i}, [a]	2.6103(13)
N(1)–Cd(1)–N(2)	70.48(15)
O(3)–Cd(1)–O(4)	54.79(15)
Cl(1)–Cd(1)–Cl(1)^{i}	84.31(4)
N(1)–Cd(1)–Cl(1)	116.89(12)
N(2)–Cd(1)–Cl(1)^{i}	160.07(12)
N(1)–Cd(1)–O(4)	142.04(15)
Cd(1)–Cl(1)–Cd(1)^{i}	95.69(4)

[a] Symmetry transformations used to generate equivalent atoms: $i = 2 - x, 1 - y, 1 - z$.

layers parallel to (1 0 −1) is lower (−100 kJ mol^{-1} per pair). Consequently, interactions between these molecular pairs stand out as structure determining, since other molecular pairs of the first coordination sphere have significantly lower stabilizing energies (< 9 kJ mol^{-1}, see Table S1, Supplementary material). A topology of the intermolecular interaction energies for the crystal structure of **1** is summarized by an energy framework [106], displayed in Fig. 2C and D.

3.3. Solution studies

NMR spectroscopy is very useful technique for determination of structure of Cd complexes in solution since existence of equilibrium of free and coordinated organic ligands [107], two mononuclear complex species [108] or binuclear/mononuclear complex species [109] can be easily recognized by increased number of signals. ^{1}H, ^{13}C and ^{113}Cd NMR spectra (Figs. S2–S4, Supplementary material) of **1** recorded in DMSO-d_6 at ambient temperature exhibit one set of ^{1}H, ^{13}C and ^{113}Cd resonances. This refers to a single ligand environment, also found in the solid state structure of **1**. Position and number of signals in ^{1}H NMR spectrum of **1** at ambient temperature remained the same even after 48 h (Fig. S2, Supplementary material). The chemical shift of the ^{1}H, ^{13}C and ^{15}N (derived from ^{1}H-^{15}N HSQC and HMBC spectra) resonances in **1** are very similar to those found in Cd(II) complex with related (*E*)-ethyl-2-(2-pyridin-2-yl-methylene)hydrazylacetate [75], which indicates that the ligand in **1** is coordinated bidentately *via* pyridine and hydrazone nitrogen atoms. A singlet at 1.80 ppm in ^{1}H NMR spectrum (Fig. S2, Supplementary material) and signals at 21.8 and 177.2 ppm in ^{13}C NMR spectrum of **1** (Fig. S3, Supplementary material) correspond to an acetate ion. When acetate is coordinated to metal ions particular deshielding of δ(^{13}C) of the carbonyl carbon is expected [110]. The downfield shift of the signal of CH_3COO in ^{13}C NMR spectrum of **1** in comparison to the signal of carbonyl carbon atom of uncoordinated acetate (171.93 ppm) [111] points to the presence of coordinated acetate. Further evidence for acetate ion coordination is derived from the NOESY spectrum of **1** wherein correlation signal of methyl group from acetate ion with methylene protons (CH_3COO/C_8H_2) was observed due to mutual spatial proximity (Fig. S6, Supplementary material). Coordination of the ester carbonyl group to Cd(II) in solution can be excluded, since there is no significant change in the chemical shift of ester carbonyl carbon atom (C9) in ^{13}C NMR spectrum of **1** in comparison to spectra of free ligands similar to aphaOMe [75].

The coordination behavior of Cd(II) is typical of a soft acid and

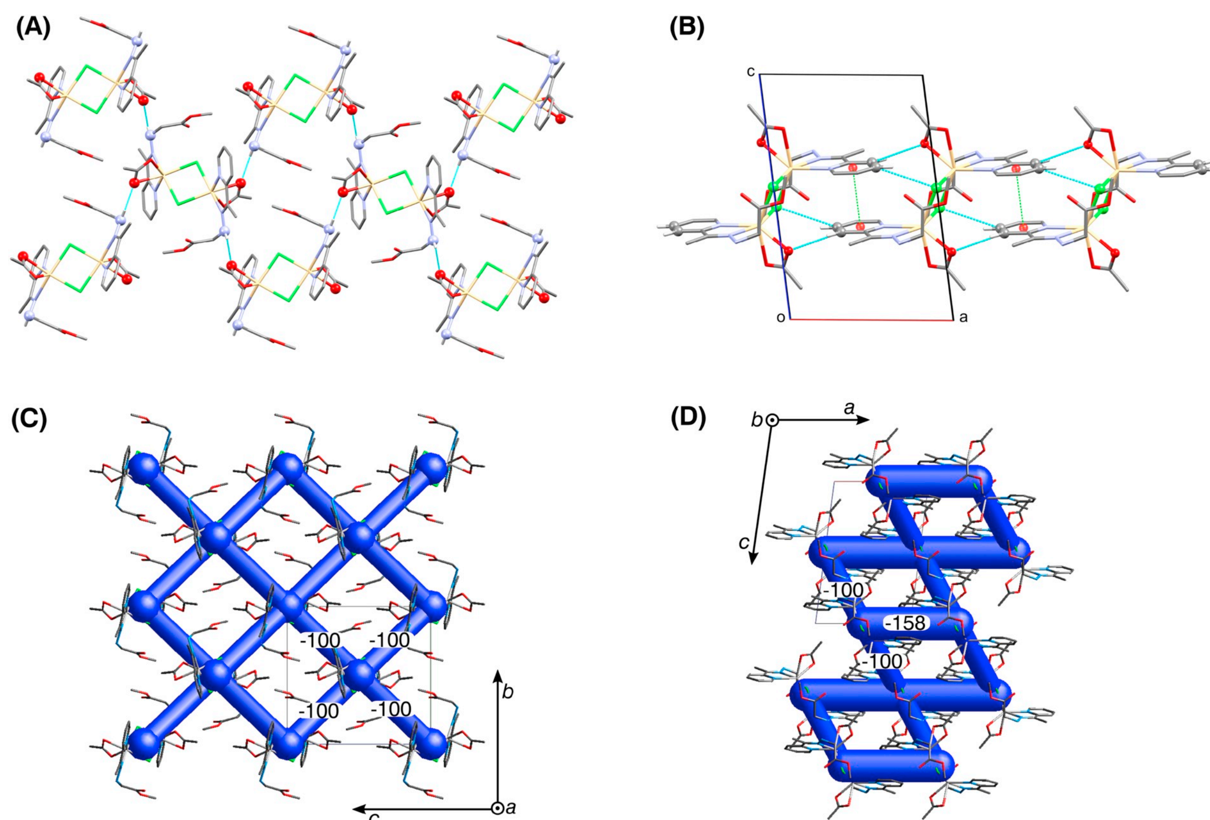

Fig. 2. Packing in the crystal structure of **1**. Hydrogen atoms, except those involved in hydrogen bonding in (A) and (B), are omitted for clarity. (A) 2D assembly parallel to (1 0 −1) generated by hydrogen bonding. (B) 1D supramolecular chain along [100] direction formed by π-π stacking interactions of pyridine rings and weak hydrogen bonds. (C) and (D): Energy frameworks for the total nearest neighbor pairwise interaction energies. The cylinders connect molecular centroids, and their thickness is proportional to the magnitude of the energy. The numbers indicate energy associated with each cylinder in kJ mol^{-1}. Pairwise energies with magnitudes < 10 kJ mol^{-1} have been omitted for clarity.

orbital diffuseness of Cd(II) acceptor atom is well matched with diffuse sulfur donor orbitals [112]. This is corroborated by the strong thiol-binding ability of Cd(II) [113]. However, sulfoxides which contain O and S donor atoms, prefer coordination *via* O atom to Cd(II) [114]. This is in line with the CSD survey where in all found X-ray structures of Cd (II) complexes a DMSO molecule was coordinated *via* O atom exclusively [96]. In presented biological experiments (*vide infra*) the stock solution of **1** in DMSO was used as a starting material for testing. To check if a DMSO molecule is coordinated to Cd(II), ^{1}H NMR spectrum of freshly prepared solution of **1** in DMSO-d_6 (0.006 M), with addition of 5% (vol.) DMSO, was recorded (Fig. S11, Supplementary material). Generally, S-bound DMSO ligands exhibit ^{1}H NMR chemical shifts approximately 1 ppm downfield relative to free DMSO (~2.54 ppm), whereas O-bound DMSO exhibits a smaller downfield shift (0.05–0.5 ppm) [115]. Since no change in ^{1}H NMR chemical shift of free DMSO was noticed, even after 24 h (Fig. S11, Supplementary material), the coordination of DMSO to Cd(II) ion in solution of **1** can be excluded.

NMR spectroscopic investigations at ambient temperature revealed evidence consistent with the presence of just one Cd(II) complex species in solution of **1**. However, existence of one set of signals in NMR spectra may also correspond to the pentacoordinated mononuclear complex obtained by the cleavage of the two chloride bridges that give rise to the dinuclear complex **1**. In order to address this issue experimentally obtained UV–Vis spectrum of **1** in DMSO (Fig. S12, Supplementary material) was compared to the calculated absorption spectra of free aphaOMe ligand, pentacoordinated mononuclear complex and dinuclear complex **1** (Fig. S13, Supplementary material). Theoretical spectrum of dinuclear species has strong absorption at 310 nm (H-1 → LUMO) with shoulder band at 265 nm (H-1 → L + 2), and shows the best agreement with the experimental data. As a consequence of change in the coordination environment, mononuclear Cd complex has additional transition at 211 nm (Fig. S13, Supplementary material). All absorptions can be assigned to the intraligand π–π* transitions as it is indicated by composition of the main molecular orbitals relevant for the electronic transitions (Fig. S14, Supplementary material).

3.4. Anticancer investigations

3.4.1. Superior pro-apoptotic activity of 1 as compared to CDDP

Pro-apoptotic activity of **1** has been assessed after 24 h incubation on MCF-7 and AsPC-1 cells by means of Annexin V/PI dual staining method. Percentages of Annexin V single-stained and double-stained cells were summarized for each concentration of investigated compound. The computed percentages were charted against corresponding concentrations and ApoC$_{50}$ concentration was computed as the one that corresponds to 50% of whole apoptotic events (early and late apoptosis) on the concentration-response curve (Fig. S15, Supplementary material). Our experimental result reveals a high incidence in apoptotic death induction and this for both cell lines (Fig. 3, Table 3). Activity of **1** is especially powerful on MCF-7 cells as at 30 μM all cells are Annexin V/PI positive (Fig. 3). AsPC-1 cells, notorious for broad-spectrum drug resistance [82,83], are responding surprisingly well to the treatment with **1** as, at 30 μM more than half of AsPC-1 cells are either in early or advanced apoptosis. Comparing current with our previously published data [99,116–118] here investigated complex **1** is the strongest inducer of apoptosis in AsPC-1 cells, including CDDP. The only metal complex that induced apoptosis in this CSC model reached significant percentage of Annexin V-stained cells only at 75 μM [99], as well as the best one referring to organic compounds [116].

As mentioned before, activity of CDDP on AsPC-1 cells has been evaluated in our previous work with a very poor outcome [116]. In the current study, CDDP reveals to be more effective on MCF-7 than AsPC-1 cells, but its pro-apoptotic activity was still less remarkable compared to **1** (Fig. 3). While more than a half of MCF-7 cells in the samples subjected to **1** at 10 μM were found as double-stained, CDDP at 75 and 100 μM guided only one third of those cells toward advanced stages of apoptotic death. Relying on results presented here and those we previously reported [116–119], **1** showed superior activity on both cell lines in respect to CDDP or other compounds investigated on CSCs.

3.4.2. Changes in cell cycle distribution indicate on DNA replication issue

The difference in intensity of apoptotic response between MCF-7 and AsPC-1 cells could be originated by either **1** striking different cellular targets in each cell line or by the fact that those cell lines from different phenotype respond in a differential mode to the same challenge. Although changes in distribution within mitotic phases cannot provide more precise information on the mechanism of drug's activity, those can at least indicate which process within the cell cycle was mostly distressed by **1**. In Fig. 4, noticeable concentration-dependent shifts in distribution of cells are observed within mitosis when MCF-7 cells are subjected to **1**. A slight accumulation in the S phase remains the dominant alteration in cells treated with 10 μM, progressing to a mitotic arrest in S phase at 30 μM. Within concentration from 50 to 100 μM, **1** induces G0/G1 blockage with a magnitude increasing in concentration-dependent manner. Such a rearrangement denotes on concentration-dependent obstructions during DNA replication.

Seemingly, treating AsPC-1 cells with **1** induces a different kind of cell cycle rearrangements as for MCF-7 cells (Fig. 4). In the AsPC-1 samples subjected to **1** at 30 μM, cells are hindered to enter the S phase, thus inducing a mild accumulation in G0/G1. At the higher concentrations (50 and 75 μM), cells are found gathered at the S-to-G2 restriction point, whereas treatment at 100 μM results in an arrest in the S phase. This time changes are accompanied by a concentration-dependent amplification of apoptotic response (Figs. 3 and 4). Cell cycle alterations seen in samples incubated with 50 and 75 μM indicate that cells passed the process of chromosomal replication but were restrained to enter the final phase of mitotic division probably due to necessary DNA repair. In cells treated with 100 μM, division is delayed during replication, which suggests that **1** induces at such concentration a damage that had to activate DNA repair mechanisms before accessing S-to-G2 restriction point.

As stated before, CDDP did not achieve any activity against AsPC-1 cells. Considering its relevance as a reference compound, cell cycle assessment has been performed and described previously [116]. Here, CDDP applied in a concentration range from 1 to 50 μM on MCF-7 cells induces a significant accumulation in G2/M phase (Fig. 4). In none of those samples the incidence of neither apoptotic nor necrotic events are notably different compared to non-treated control (Fig. 3). Significant augmentation in frequency of Annexin V-stained cells is found in the samples subjected to CDDP at the highest concentrations (75 and 100 μM) with both of them shifting cells to stop in S-to-G2 restriction point. CDDP is known for its ability to trigger various mechanisms that affect homeostasis and lead to apoptosis, with liable formation of DNA lesions [120–124]. Initially, such type of results were reported as exclusively depended on p53 status and drug concentration [125–129]. According to those reports, in cells protected with mutated p53, arrest at the G2 phase was found as the dominant characteristic, while increase in CDDP concentration induced cell cycle block in the S phase. On the contrary, in cells with wild-type (*wt*) p53, arrest in the G1 phase was found at all concentrations of CDDP. Later on, it was disclosed that CDDP induces arrest in the S phase in a p53-independent manner [130]. Nevertheless, He et al. [131] recently revealed that such type of cell cycle arrest strongly depends on pathways activated by particular DNA damaging agents, including CDDP, rather than on the p53 status of treated cells. MCF-7 cells used here are reported to have *wt* p53 status [132], which is not the case of AsPC-1 cells [133]. Thus, distribution of cells within mitotic division in MCF-7 samples afterwards treatment with CDDP (Fig. 4) correspond to previously described data [131]. The divergence in cell cycle response of MCF-7 cells to **1** and CDDP treatments can be addressed to different types of interference those two drugs induce during DNA replication. On the other hand, alterations in

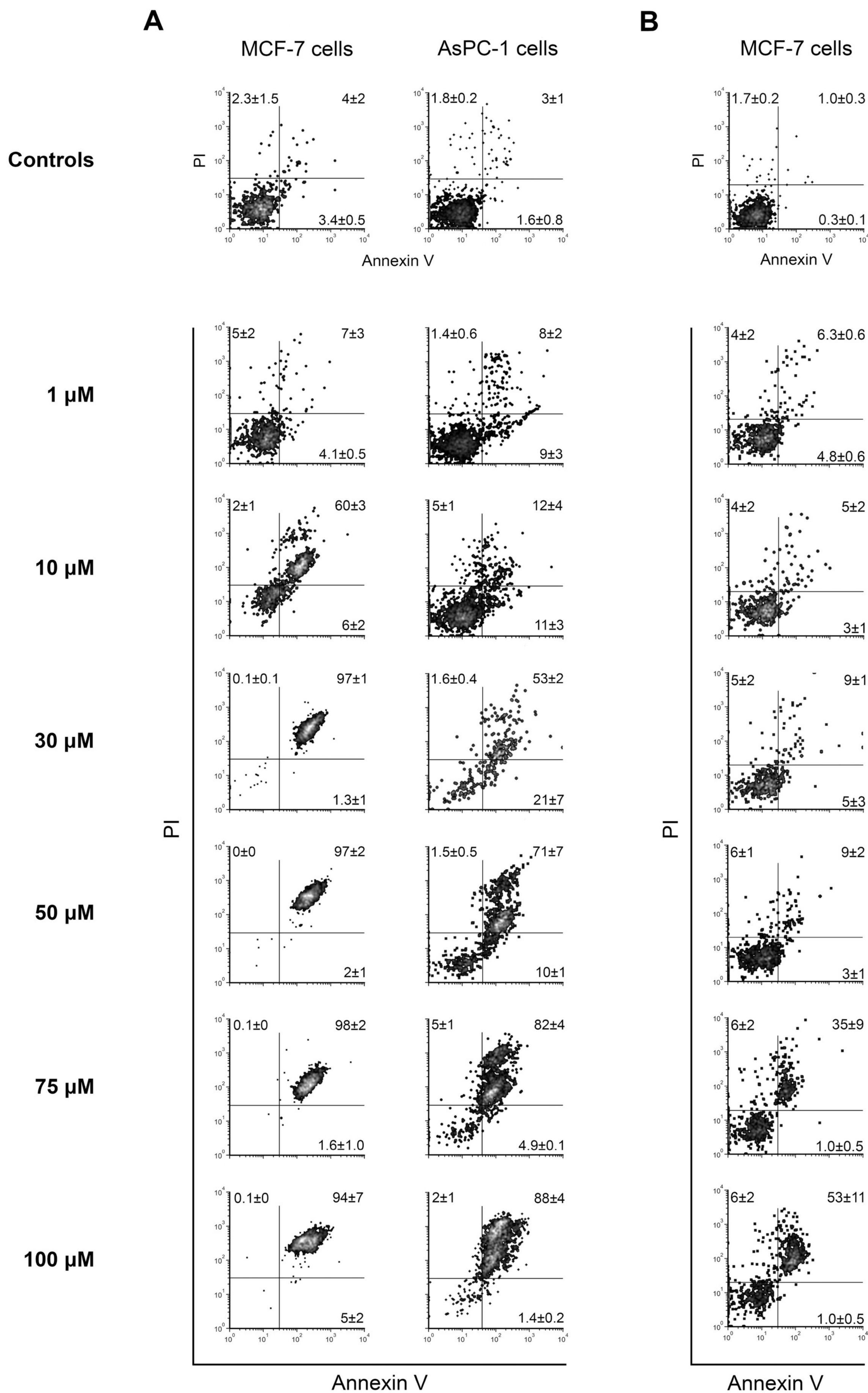

(caption on next page)

Fig. 3. Incidences of apoptotic and necrotic deaths in cells treated with **1** (A) and CDDP (B) determined after 24 h incubation by means of Annexin V/PI dual staining method. In Annexin V/PI dot plots cells are discriminated as viable (non-stained cells, lower left quadrant), cells in early phase of apoptosis (Annexin V single-stained cells, lower right quadrant), cells in advanced phases of cell death of apoptotic death (double-stained cells, upper right quadrant), and necrotic cells (PI single-stained cells, upper left quadrant). Results are represented as the mean ± SD percentages of two replicates from independent experiments.

Table 3
Computed $ApoC_{50}$ values for **1** and CDDP according results of Annexin V/PI double staining method after 24 h incubation.

Compound	$ApoC_{50}$ [μM]	
	MCF-7	AsPC-1
1	8.3 ± 1.4	20 ± 2
CDDP	85 ± 52	n.d.[a]

[a] n.d. - not determined as no activity was observed in the concentration range 1–100 μM.

cell cycle distribution of MCF-7 and AsPC-1 cells due to the treatment with **1** indicate that both cell lines experienced distress during DNA duplication, while their phenotypic particularities most probably were accountable for initiation different check points, thus leading to diverse distribution of cells during mitosis. However, if present results indicate that **1** induces cell cycle shifts different than for CDDP, thus determination whether **1** has the ability to establish a strong interaction with DNA or is involved in a mechanism involved in the regulation of the DNA replication phase remains to be elucidated.

*3.4.3. Compared to CDDP, apoptosis induced by **1** reveals as lower caspase-dependence with possible interruption in activation of extrinsic pathway*

To determine the role of caspases activation in process of apoptotic death due to **1**, impact of Z-VAD-fmk pan-caspase inhibitor on initiation and evolution of cell death was monitored, as was the activation of either caspase-8 or -9 after 6 h incubation of **1** at $ApoC_{50}$ concentration. As represented in Fig. 5A, apoptotic death shows low caspase-dependency in both cell lines (17 ± 2% and 25 ± 1% for MCF-7 and AsPC-1 cells, respectively). While co-incubation with Z-VAD-fmk has almost equivalent consequence on initiation of apoptotic death (28 ± 7% and 22 ± 3% in MCF-7 and AsPC-1 cells, respectively), evolution of apoptosis in MCF-7 samples was nearly irrespectively due to caspases' activity (11 ± 1%) contrary to AsPC-1 cells (32 ± 11%). According to those data, it is obvious that apoptosis induced by **1** is partially caspase-dependent in both treated cell lines [134]. Additionally, pan-caspase inhibition yielded significant augmentation of necrotic events (41 ± 8% and 67 ± 2% in MCF-7 and AsPC-1 cells, respectively), which is an expected consequence of interrupted apoptotic cascades [38].

Moreover, when treated with **1**, both cell lines display strikingly suppressed activation of caspase-8 (Fig. 5B) and not for caspase-9. While for MCF-7 percentages of cells with single activated caspase-9 or both activated caspases were at the level of non-treated controls, modestly stimulated activation of caspase-9, accompanied by significant decrease in cross-talk activation of extrinsic pathway, was the prominent finding for AsPC-1 cells. Such noticeable decline in active form of caspase-8, even below basal levels in both cell lines, connotes a possibility that **1** may directly interfere with the process of caspase-8 activation.

Considering that the cell cycle changes in both cell lines treated with **1** indicate a disturbed DNA replication process (Fig. 4), possible role of caspase-2 remains to be investigated during further studies [135].

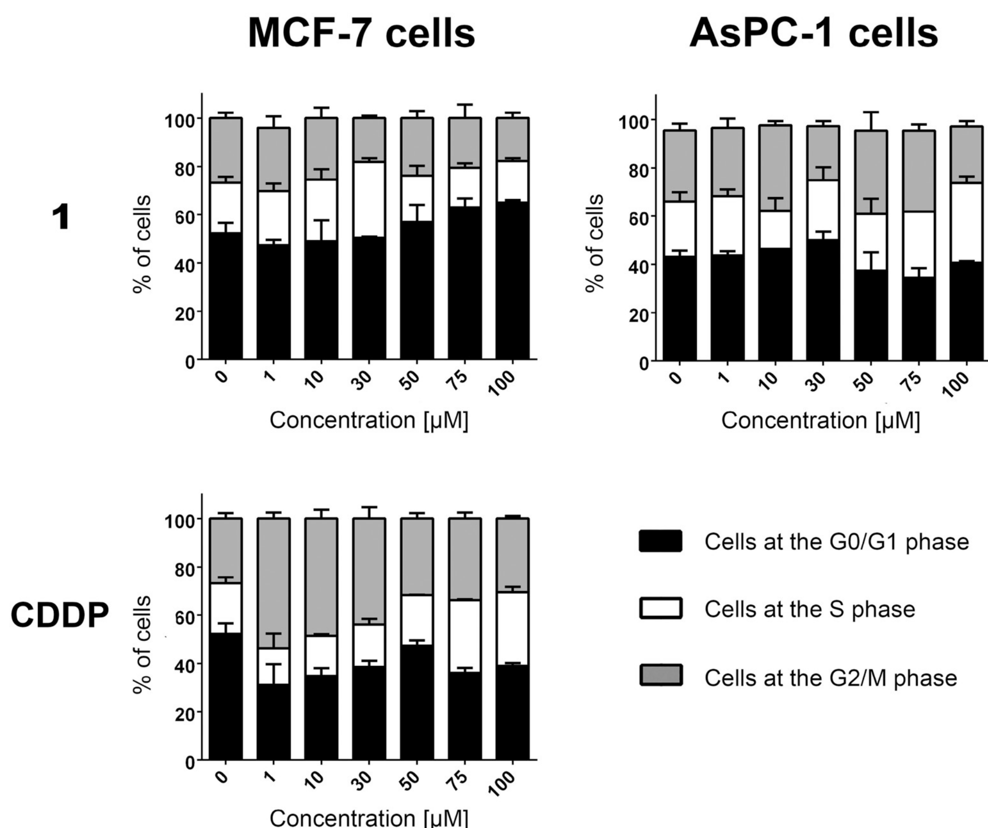

Fig. 4. Distribution of cells within phases of mitotic division afterwards 24 h incubation with **1** and CDDP. Results are represented as the mean ± SD percentages of two replicates from independent experiments.

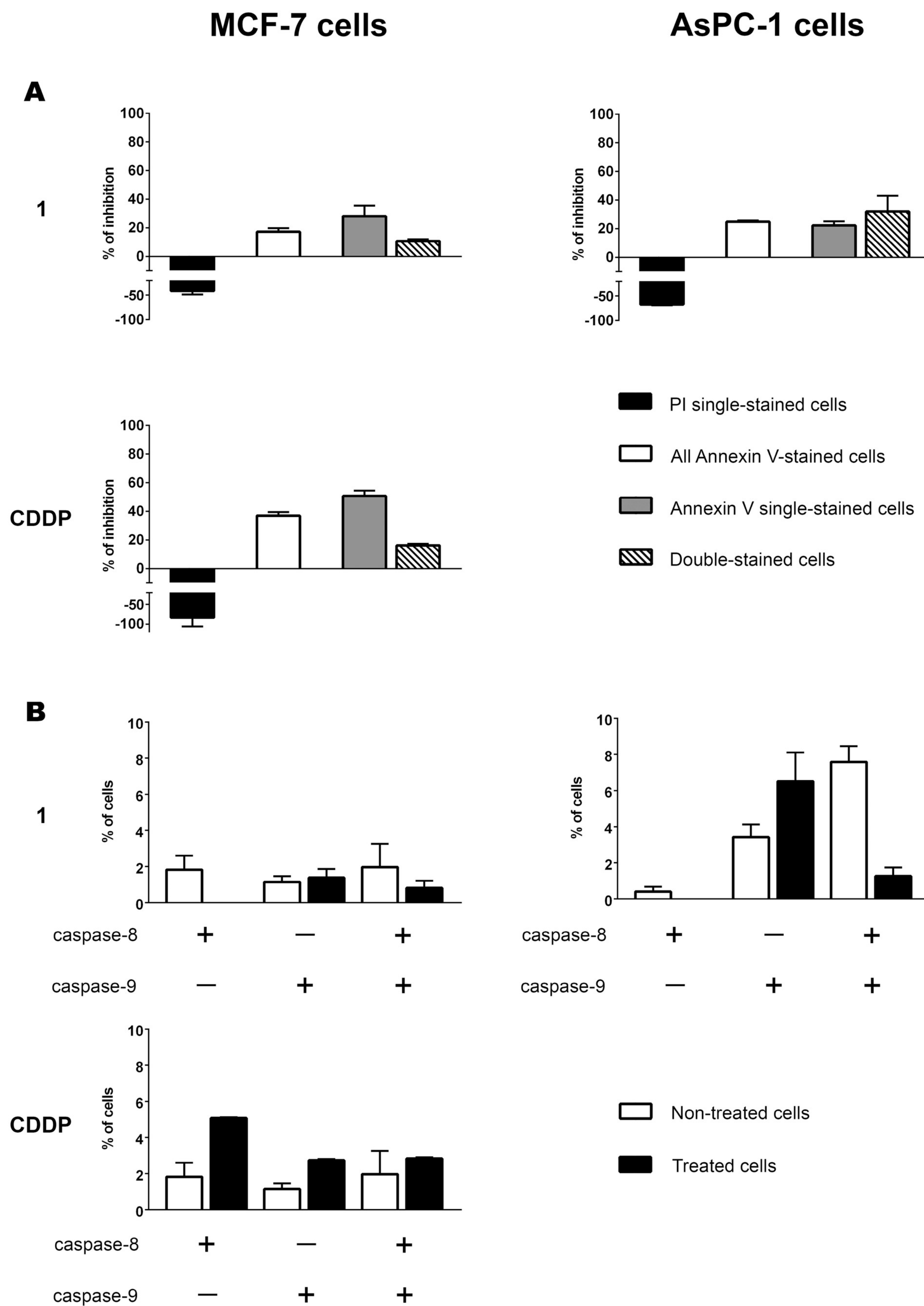

Fig. 5. Caspase-dependency of cell death determined over percentages of cell death inhibition after co-incubation with pan-caspase inhibitor with investigated compounds applied at their $ApoC_{50}$ concentration (A). Analyses are done after 6 h treatment by means of Annexin V/PI double staining method. Results are expressed as the mean ± SD of two replicates from independent experiments. Percentages of positive for activated caspase-8, caspase-9 or both caspases determined after 6 h incubation with investigated compounds applied at their $ApoC_{50}$ concentrations (B). Results are represented as the mean ± SD of two replicates from two independent experiments.

Since CDDP did not induce cell death in AsPC-1 samples, caspase-dependency of apoptosis triggered with this compound was evaluated on MCF-7 cells only. Apoptotic death induced by the treatment with CDDP revealed as more caspase-dependent compared to that caused by **1**, with very similar caspase-dependency pattern regarding early and advanced phases of apoptosis evolution between these two treatments (Fig. 5A). In MCF-7 samples subjected to CDDP, activation of caspase-8 was the dominant event, accompanied with modestly activated caspase-9 and cross-talk pathways interaction at the level of non-treated control (Fig. 5B). This result aditionally demonstrates that **1** and CDDP do not share analogous mode of action.

*3.4.4. Complex **1** is a strong inducer of mitochondrial superoxide generation*

According to previously published research on putative mode of metal complexes activity [136], cadmium-based small molecules preferentially interfere with nucleic acid metabolism, membrane function and induce metabolic stress. As reviewed above, current results on alterations in cell cycle distribution indicate that **1** interfered DNA replication process. In addition, it was reported that Cd(II) complexes have the ability to induce apoptosis through the generation of reactive oxygen species (ROS) [137]. Although ROS-producing ability is well known mechanism of Cd(II) toxicity [138,139], this particular feature cannot be instantly attributed to its complexes with organic ligands. However, such evidence motivated us to evaluate the potential of **1** to trigger superoxide ($O_2\cdot^-$) production in mitochondrion, knowing this organelle is the key source of intracellular ROS [140]. The extent of $O_2\cdot^-$ accumulation, as the primarily yielded mitochondrial ROS, depends on the balance between rate of $O_2\cdot^-$ generation and rapidity of its conversion toward hydrogen peroxide by means of superoxide dismutase (SOD) enzyme. Furthermore, extent of $O_2\cdot^-$ generation depends on the concentration of the enzyme containing electron carrier, concentration of electron donor, and the second–rate order constants for the reaction between them [141]. There are two intracellular isoforms of SOD: SOD1 that is located in cytoplasm and intermembrane mitochondrial space, while SOD2 is situated exclusively within mitochondrion matrix [140]. It was previously demonstrated that both AsPC-1 and MCF-7 cells have lower expression levels of SOD2 compared to healthy controls [142,143]. Contrary to AsPC-1, MCF-7 cells additionally have reduced level and activity of mitochondrial SOD1 [143], together with significantly higher extent of uncoupled respiration in respect to normal breast epithelial cells MCF10A [141,144].

Current experiments are run in a way that acknowledges the difference in susceptibility of those two cell lines to ROS-producing agents described above. Concentrations of **1** at 50 μM for MCF-7 cells and 75 μM for AsPC-1 cells were chosen considering both are situated on the top plateau of the corresponding concentration-response curves (Fig. S15, Supplementary material). ROS-generating properties of CDDP, as a reference compound, are assessed using the same concentrations, even on AsPC-1 cells albeit CDDP was previously confirmed as unable to induce cell death in the 2D CSC model after 24 h of treatment [116]. Incubation with **1** significantly increases the percentage of $O_2\cdot^-$ producing cells in both AsPC-1 and MCF-7 cells (Fig. 6). As expected, the median quantity of $O_2\cdot^-$ per cell is greater in MCF-7 samples, with a 2.7-fold increase in median fluorescent intensity (MFI) values, compared to a 1.2-fold of MFI rise in AsPC-1 treated cells. CDDP revealed lower proficiency in generating $O_2\cdot^-$ in MCF-7 cells compared to **1**, although it significantly increased size of $O_2\cdot^-$ positive subpopulation with gain in MFI values of 1.8-fold than control. Surprisingly, the average percentage of AsPC-1 cells positive for mitochondrial $O_2\cdot^-$ after CDDP treatment remains at the level of non-treated controls, while the MFI values are even below untreated cells.

ROS originated in mitochondria, rather than from other intracellular sources, are confirmed as one of the most pathogenic factors when the rate of their production exceeds the homeostatic level [145,146]. And enhanced mitochondrial ROS production leads to mitochondrial permeability transition pore (mPTP) opening with consequential dissipation of mitochondrial transmembrane potential (MTP) and initiation of cell death [140]. Collapse of MTP represents instant change in permeability of the inner mitochondrial membrane that permits to molecules of a size up to 1.5 kDa to go through the membrane. The following course of events includes interruption of ATP synthesis, mitochondrial swelling, and initiation of cell death. In order to evaluate if enhanced generation of $O_2\cdot^-$ due to treatments with **1** and CDDP induces mPTP opening, we assessed the MTP status in treated cells.

In AsPC-1 cells treated with **1**, out of 44 ± 3% were positive for Annexin V and/or 7-AAD, 36 ± 2% of them were positive for altered MTP (Fig. 7). Furthermore, among cells with no signs of changed MTP status, 9.7 ± 0.4% were positive for Annexin V and 5.6 ± 0.8% were stained with 7-AAD. Amidst 59 ± 4% of 1-treated MCF-7 cells that underwent cell death, 54 ± 5% were positive for dissipated MTP, whereas 5 ± 1% and 5.2 ± 0.1% of those with intact MTP were stained with Annexin V or 7-AAD, respectively (Fig. 8). Thus, the remarkable difference regarding percentages of $O_2\cdot^-$ generating cells and MFI values between AsPC-1 and MCF-7 cells (Fig. 6), denotes a distressed mitochondrial function and integrity (Figs. 7 and 8).

With reference to $O_2\cdot^-$ production in CDDP-treated AsPC-1 samples (Fig. 6), it was expected the same treatment would not cause significant impact on MTP (Fig. 7). However, it could not be predicted that CDDP acted as MTP stabilizing agent, decreasing incidence of spontaneously developed alteration of MTP seen in non-treated AsPC-1 cells. Yet the same phenomenon was found in MCF-7 cells subjected to CDDP (Fig. 8). While half of MCF-7 cells treated with CDDP were positive for increased $O_2\cdot^-$ with almost twice-greater MFI, percentage of cells with dissipated MTP was also below those of non-treated samples like for AsPC-1. Recently, Marullo et al. [120] showed that mitochondrial ROS generation is another important mechanism responsible for anticancer activity of CDDP yet not well characterized previously. In their work, significant increase in mitochondrial $O_2\cdot^-$ levels starts after 16 h of CDDP treatment indicating that time course of $O_2\cdot^-$ production is consistent with a reduced synthesis of electron transport chain proteins due to formation of adducts with mitochondrial DNA [147]. Therefore, according to previously postulated mechanism, increased extent in mitochondrial $O_2\cdot^-$ is rather delayed, as a consequence of disrupted protein synthesis, instead of an early event caused by pro-oxidant activity of CDDP. This is not in agreement with our observation in MCF-7 cells (Fig. 6). Since in the current investigation CDDP is employed only as a reference compound, further discussion on possible mechanisms underlying elevated mitochondrial $O_2\cdot^-$ formation while preserved MTP (Figs. 6–8), would be beyond the scope of our study. Final remark concerns the obvious difference in mechanisms of activity between CDDP and investigated cadmium complex at the mitochondrial level.

*3.4.5. Complex **1** shows a mighty activity on 3D CSC models*

Significance and advantages of drug activity testing on 3D models compared to 2D cultures have been reviewed previously [117,147]. Here, we tested activity of **1** on AsPC-1 and MCF-7 3D cultures over 8 days treatment time, with CDDP as a reference drug. Gained results provide an excellent illustration of inconsistency between drug's effects obtained on 2D and 3D models, additionally emphasizing the importance that use of *in vitro* tumors has for more accurate validation of preclinical drug development [148,149]. While **1** in 2D MCF-7 model displayed vigorous pro-apoptotic activity already at 10 μM (Fig. 3), it achieved growth inhibition of MCF-7 spheroids only at the highest applied concentration of 100 μM (Figs. 9 and 10). While treatment with **1** at 1 μM did not show any effects, at 10 μM a modest activity with a 2.1 ± 0.1-fold in size increase as compared to 2.5 ± 0.3-fold in non-treated control on day 8.

For CDDP, examined on MCF-7 3D model previously [150], the current study confirms its ability to reduce initial size of treated spheroids at concentrations of 10 μM (0.85 ± 0.04-fold) and 100 μM

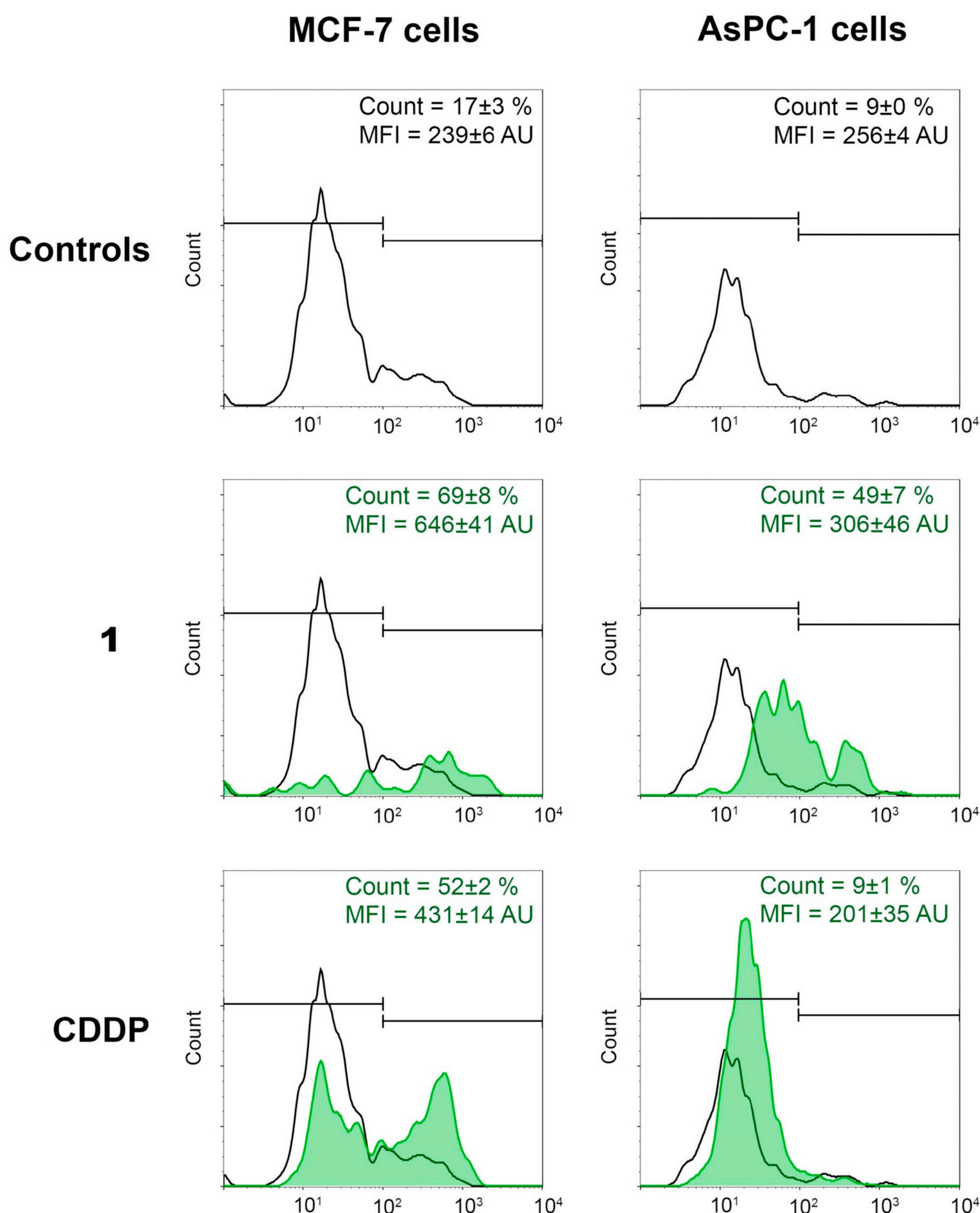

Fig. 6. Mitochondrial superoxide ($O_2\cdot^-$) generation determined after 6 h treatment with investigated compounds applied at 50 μM (MCF-7 cells) and 75 μM (AsPC-1 cells). Analyses have been performed by means of MitoSox Red staining. Results are represented as percentages of cells positive for $O_2\cdot^-$ production and over median fluorescent intensity (MFI) expressed in arbitrary units (AU) computed for $O_2\cdot^-$-positive subpopulation. All results are represented as the mean ± SD of two replicates from 3 independent experiments.

(0.81 ± 0.05-fold). Nevertheless, results on AsPC-1 spheroids disclose an interesting similarity in pattern of **1** and CDDP activities (Figs. 9 and 11). As reviewed above, CDDP does not induce cell death in AsPC-1 2D cells over 24 h of incubation [116]. On the contrary, CDDP against AsPC-1 3D model displays an activity at all 3 tested concentrations (Figs. 9 and 11). In samples subjected to CDDP at 100 μM, extreme regression in size is recorded (0.4 ± 0.1-fold on the day 8). CDDP at 10 μM suppresses growth of spheroids (1.0 ± 0.1-fold on the day 8), while tumors treated with 1 μM record a growth of 1.4 ± 0.1-fold. Opposite to results on MCF-7 3D model, **1** was more effective on AsPC-1 tumors than CDDP (Figs. 9–11). Complex **1** at 100 μM interrupted spheroidal assemblage quite promptly after its addition on AsPC-1 3D tumors (Fig. 11). Initially, such a process produced erroneous impression of gain in size, while after 6 days of treatment spheroids are completely destroyed. In those samples, residual clustering of cells could be observed, but those formations were less compact compared to the one seen after CDDP treatment at the same concentration. The reason why the disintegration of the spheroidal structure appears so quickly after **1** was added, as AsPC-1 tumors, may be due to its pro-apoptotic activity, but the possibility that **1** induces CSCs phenotype reprogramming with consequential loss of cells' ability to congregate remains to be further investigated.

3.5. DNA binding studies

As reviewed above, results of the current biological assessment in both AsPC-1 and MCF-7 cells treated with **1** revealed that the mechanism of this compound's activity is most probably related to derangement of DNA replication process. However, the differences in cell cycle changes at the first place, together with variable pattern in caspases activation and MTP dissipation between **1** and CDDP, strongly implied that those two compounds do not interrupt cellular homeostasis

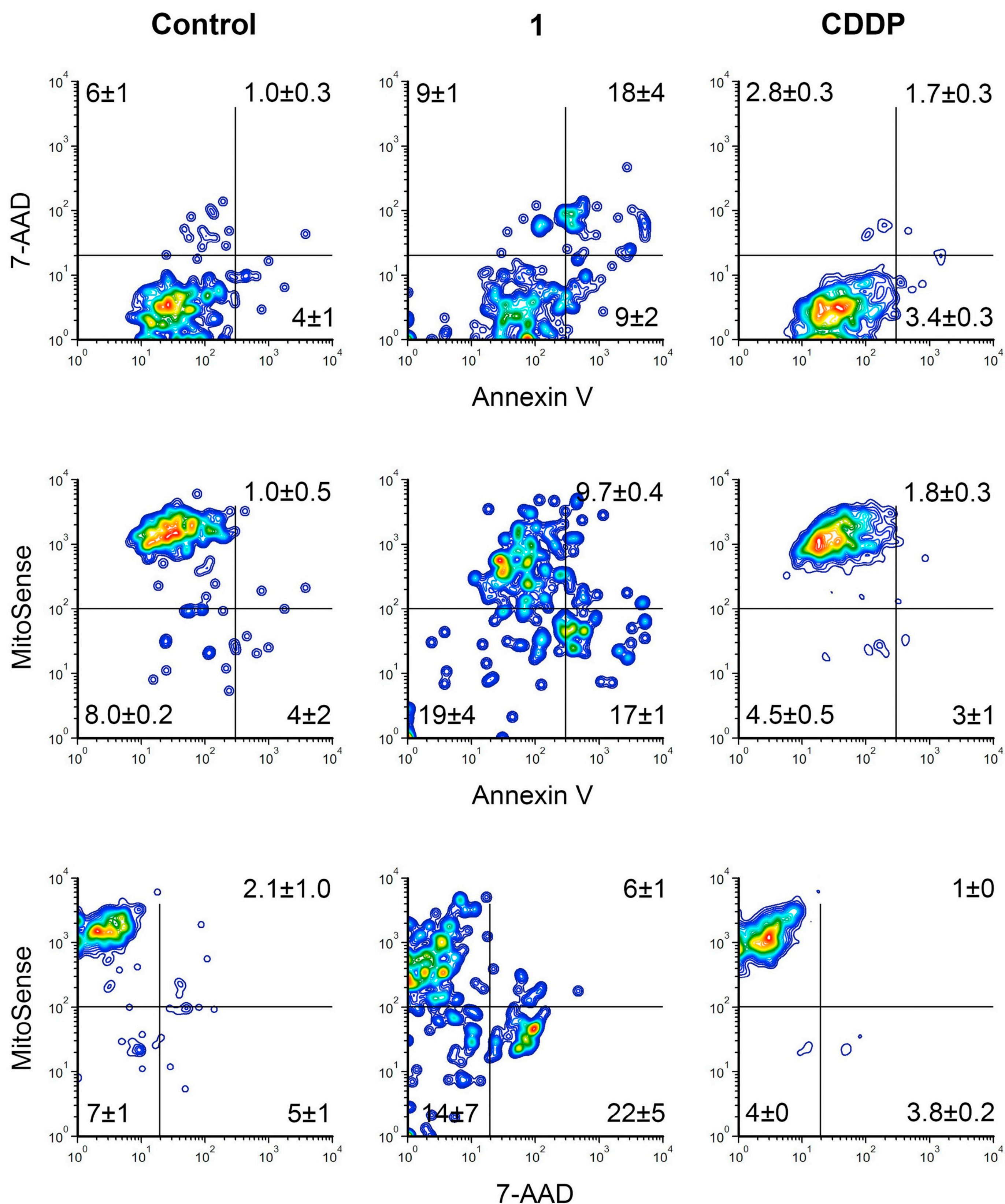

Fig. 7. Dissipation of mitochondrial transmembrane potential (MTP) in non-treated and treated AsPC-1 cells after 6 h incubation with investigated compounds applied at 75 μM. In the upper panels cells are discriminated according to the type of cell death (non-stained viable cells and stained with Annexin V and/or 7-AAD). In the middle panels cells are discriminated according to staining with MitoSense Red dye (negative cells in lower left and right quadrants have scattered MTP) and concomitant staining with Annexin V (apoptotic cells in upper right and lower right quadrants). In the lower panels cells are discriminated according to staining with MitoSense Red dye and concomitant staining with 7-AAD (cells in necrosis or advanced phase of apoptosis in the upper right or lower right quadrants). All results are represented as the mean ± SD percentages of two replicates from three independent experiments.

Journal of Inorganic Biochemistry 190 (2019) 45–66

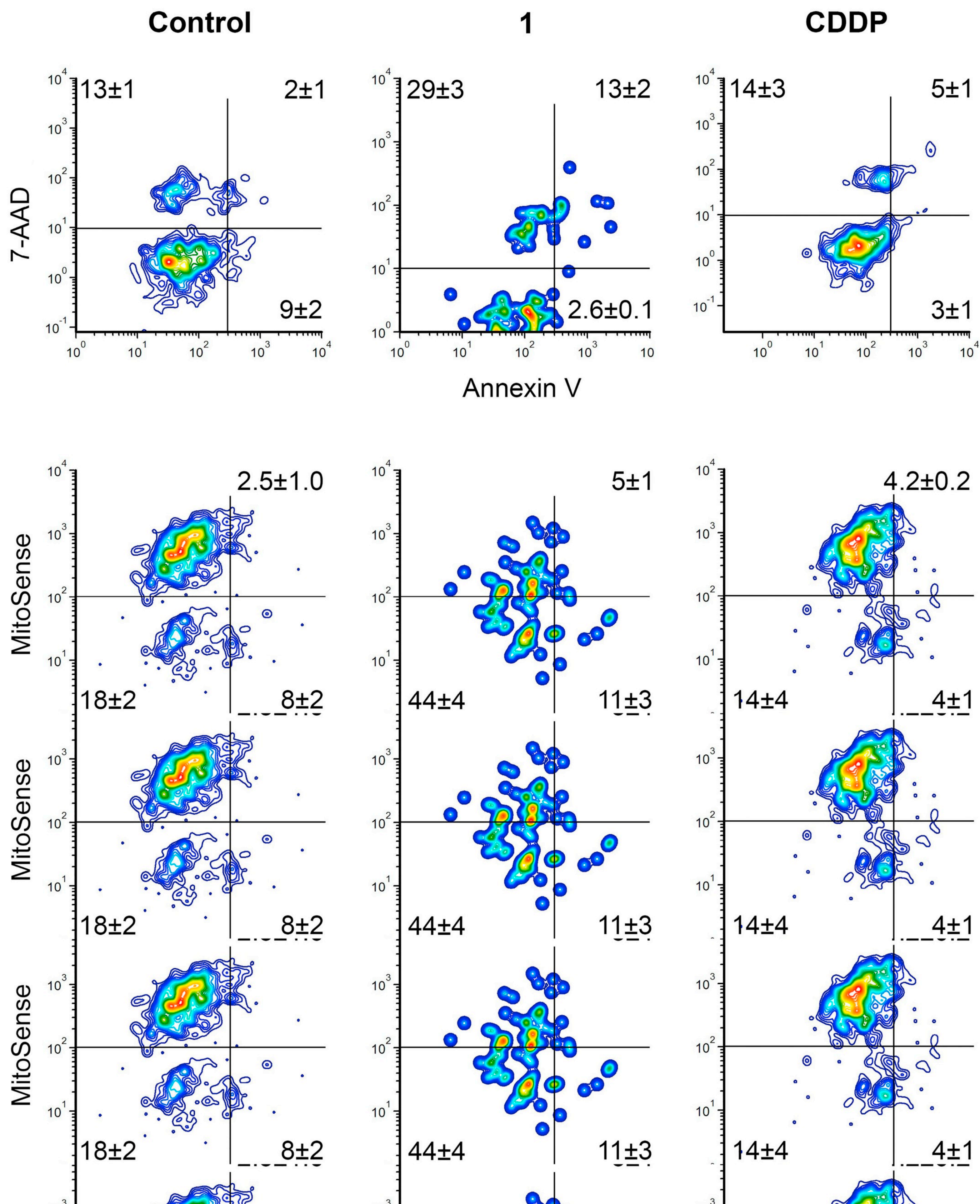

Fig. 8. Dissipation of mitochondrial transmembrane potential (MTP) in non-treated and treated MCF-7 cells after 6 h incubation with investigated compounds applied at 50 μM. In the upper panels cells are discriminated according to the type of cell death (non-stained viable cells and stained with Annexin V and/or 7-AAD). In the middle panels cells are discriminated according to staining with MitoSense Red dye (negative cells in lower left and right quadrants have scattered MTP) and concomitant staining with Annexin V (apoptotic cells in upper right and lower right quadrants). In the lower panels cells are discriminated according to staining with MitoSense Red dye and concomitant staining with 7-AAD (cells in necrosis or advanced phase of apoptosis in the upper right or lower right quadrants). All results are represented as the mean ± SD percentages of two replicates from three independent experiments.

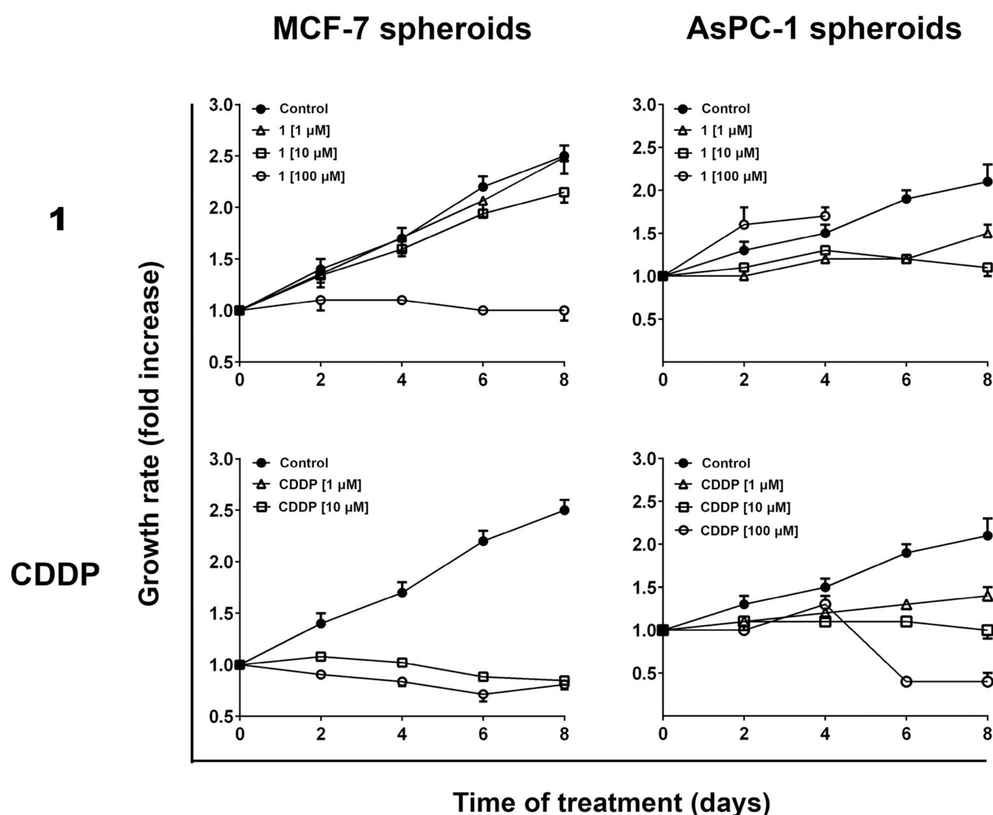

Fig. 9. Growth rate graphs for MCF-7 and AsPC-1 spheroids, non-treated and treated with investigated compounds. Results are represented as the mean ± SD fold change of two replicates from independent experiments.

in a similar way. According to those facts, it was of interest to further examine whether direct interaction of **1** with the DNA might be addressed as the cause for initiation of apoptotic death in both treated cell lines.

DNA has been generally accepted as a major pharmacological target of the majority of metal-based drugs [10]. Transition metal complexes can bind to DNA *via* both covalent and/or non-covalent interactions. In general, covalent interactions include coordination to DNA base, sugar and phosphate moieties, as well as their nuclease activity. In the case of non-covalent interactions, metal complexes the most frequently interact with DNA *via* minor groove, and by intercalation [119]. Detection of interactions of DNA with potential drugs includes variety of conclusive electrochemical and spectroscopic methods [151,152]. Among these methods, simple gel-electrophoresis experiments can give information about possible covalent interactions with DNA, while fluorescence spectroscopy competitive experiments are useful to detect non-covalent interactions and distinguish between intercalative and minor groove mode of binding [10].

Result of gel electrophoresis experiment could be a retardation of the migration of plasmid DNA through the gel, which is an indication of covalent binding [119], or change in the ratio of different forms of DNA (supercoiled, nicked circular and linear), which further indicates nuclease activity of investigated compound [10]. On the other hand, experiments which detect changes in the emission spectra of CT-DNA and two different dyes EB (a typical DNA intercalator) or H (a minor groove binder) upon addition of investigated compound are useful to distinguish between intercalation and minor groove binding [116]. It is known that EB emits intense fluorescent light in the presence of DNA due to its strong intercalation between adjacent base pairs [153]. H binds strongly and selectively with high affinity to double-stranded B-DNA structure and, like other minor groove binders, it recognizes at least four AT base pairs. It binds by combination of hydrogen bonding, van der Waals contacts with the walls of the minor groove, and electrostatic interactions between its cationic structure and the DNA [154]. In both cases the extent of the fluorescence quenching of these two dyes by competitive displacement from DNA is a measure of the strength of the interaction between investigated compound and DNA.

3.5.1. Gel electrophoretic study of interaction between 1 and plasmid DNA

The interaction of plasmid pUC19 and **1** was analyzed by agarose gel electrophoresis (Fig. S16, Supplementary material). In the presence of the increasing concentration of **1**, changes in intensity of fluorescence of EB and super-coiled form and open circular form were observed in comparison to the control (lane 1, Fig. S16, Supplementary material). The increased concentration of **1** produced quenching of fluorescence of plasmid pUC19 and no changes in band mobility. No strand scission was observed at concentration up to 0.04 mM (lanes 2–5, Fig. S16, Supplementary material). The results show that nuclease activity and covalent interaction with DNA do not present a mode of action of **1**.

3.5.2. Fluorescence study of interaction between 1 and linear DNA

Since **1** did not emit luminescence upon excitation at $\pi \rightarrow \pi^*$ transitions, both in DMSO or in the presence of CT-DNA, it was possible to obtain indirect evidence for its binding mode by fluorescent displacement experiments with EB and H dyes. Binding of EB to CT-DNA was followed by excitation at 500 nm with maximum in fluorescence at 600 nm, while experiments using H dye were followed by excitation at 350 nm with maximum in fluorescence at 444 nm. The emission spectra of EB bound to CT-DNA in the absence and presence of **1** are given in Fig. 12A. With increasing concentration of **1** (up to 20 μM), a continuous decrease in fluorescence intensity at 600 nm for EB–CT-DNA was observed (Fig. 12A). The complex quenches the fluorescence probe with the maximal decrease in the fluorescence intensity of the EB–CT-DNA by 19%, followed by saturation at high concentration of **1** (18 μM) (Fig. 12A and the inset). However, since the emission intensity of

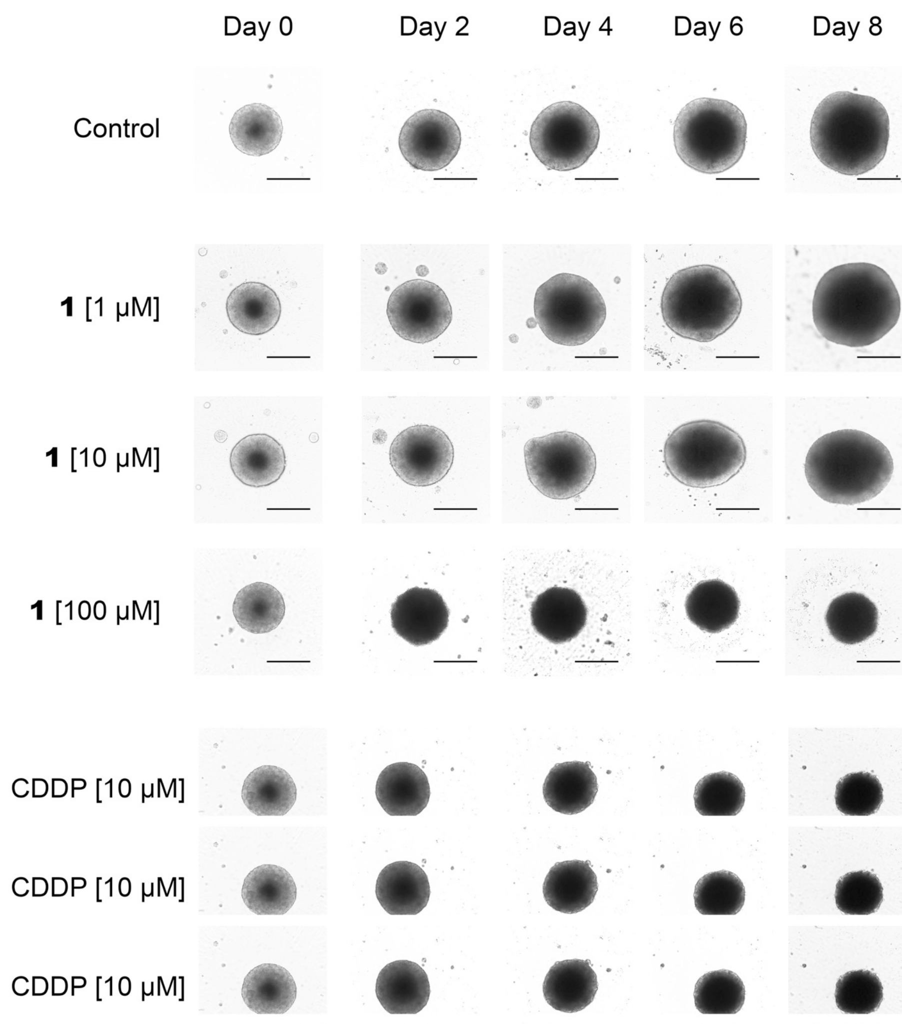

Fig. 10. Changes in size and morphology of MCF-7 3D spheroids over the 8 days of treatment with investigated compounds. Images have been taken every other day on Celigo imaging cytometer using Celigo software. Scale bar: 200 μm.

EB–CT-DNA system upon addition of **1** does not decrease > 50%, which is generally accepted threshold value if compound interacts with DNA by intercalation [155], it can be concluded that **1** binds to DNA in a different mode from EB.

Fig. 12B shows the characteristic emission spectrum of H when it is bound to CT-DNA. The addition of **1** caused appreciable reduction in the fluorescence intensity of H–CT-DNA system in a concentration dependent manner. The quenching of H–CT-DNA showed an initial saturation at 10 μM concentration of **1** (inset in Fig. 12B). It is important to note that the fluorescence intensity was reduced to nearly half of the initial value at this concentration of **1**. The half-reciprocal plot of the quenching data according to Stern-Volmer (see Supplementary data) resulted in a linear plot (Fig. 12C) with a quenching constant K_{sv} = 3.27. The value is comparable with competition similar values obtained with other metal complexes binding to minor groove [156]. With increasing concentration of **1**, an additional decrease in fluorescence intensity was observed, followed by saturation in competitive displacement from H–CT-DNA system. The decrease of H-CT-DNA fluorescence intensity was 63% with maximal applied concentration of **1**. The obtained results of the extent of the fluorescence quenching of EB by competitive displacement from EB–CT-DNA system and groove binder H from H–CT-DNA system demonstrated that **1** is a minor groove binder.

The DNA interaction study show non-covalent low binding strength of **1** into DNA minor groove together with the lack of DNA cleavage in pUC19 experiment. The changes in cell cycle distribution signify that **1** interferes in the process of DNA replication, while comparative analysis indicates that its mechanism of action differs from the one of CDDP (*vide supra*). Taking into account the high affinity of Cd(II) for S ligands, like thiol groups of enzymes and proteins [113], possible molecular target of **1** is rather related to protein(s) involved in the control of replication than DNA itself.

*3.5.3. Molecular docking of **1** with DNA*

Molecular docking showed that the compound **1** preferentially binds to the minor groove of DNA (Fig. 13). Out of 20 docking solutions, the best 12 positioned compound **1** near or into the minor groove, and only 3 solutions placed compound **1** in the major groove. Compared to the HSA binding (*vide infra*), the ChemPLP docking score for **1**-DNA interaction was significantly smaller (−52.67 compared to −83.50; Table S2, Supplementary material). This is in line with the experimental findings that **1** binds with higher affinity to the proteins (HSA, *vide infra*) than to DNA.

3.6. Acute lethality assay

As a preliminary toxicity screening, *in vivo* acute lethality of **1** and reference compound CDDP were tested on brine shrimp *Artemia salina* after 24 h incubation. LC_{50} value for complex **1** (0.316 ± 0.007 mM) was significantly higher than for CDDP (0.006 ± 0.004 mM), which

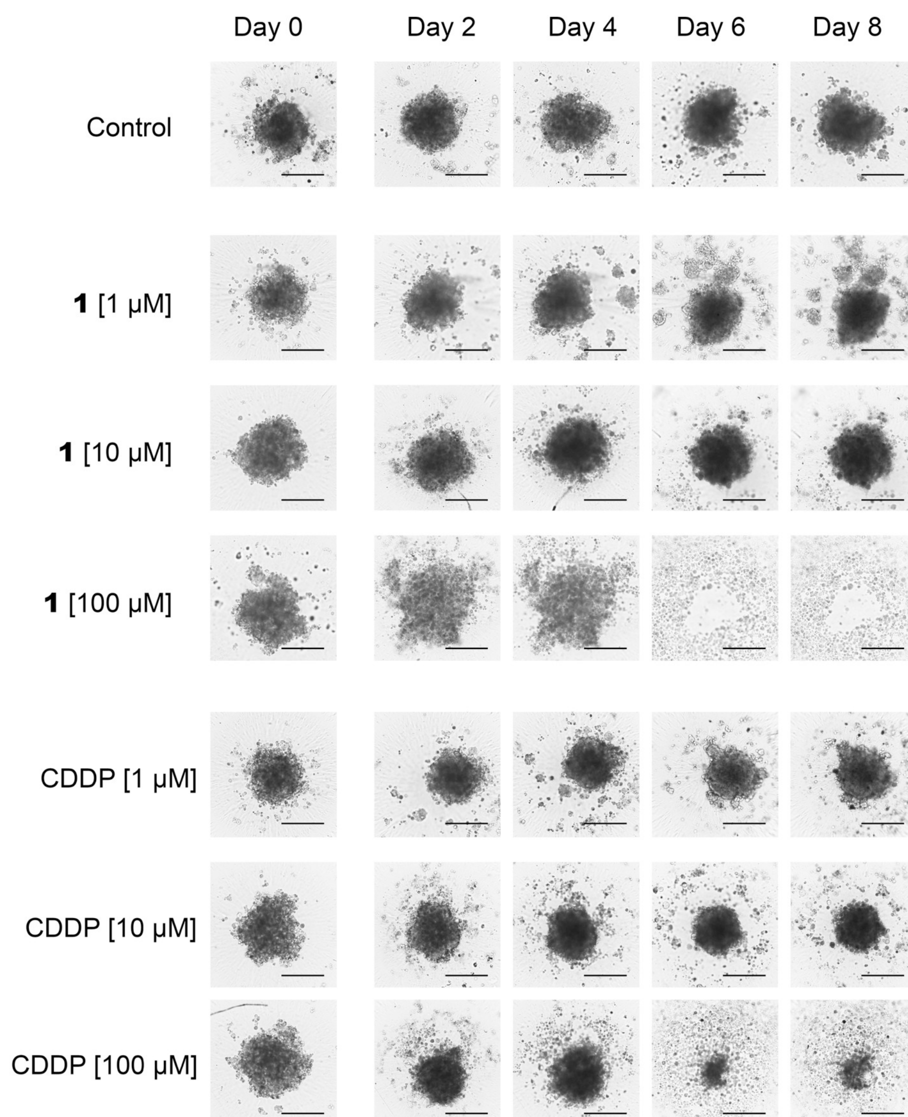

Fig. 11. Changes in size and morphology of AsPC-1 3D spheroids over the 8 days of treatment with investigated compounds. Images have been taken every other day on Celigo imaging cytometer using Celigo software. Scale bar: 200 μm.

indicates that CDDP induced higher incidence of lethality in comparison to **1**. Since that there is a good correlation between the results of LC_{50} obtained in the current bioassay and the results of the Acute Oral Toxicity Assay in Mice [157], it can be anticipated that **1** would possess the lower acute toxicity in comparison to CDDP.

3.7. Interaction with HSA

3.7.1. Experimental study of interaction between 1 and HSA

HSA is well known for its binding capacity and repository for an extraordinarily diverse range of molecules which makes it an important factor in the pharmacokinetic behavior of many drugs by affecting their efficiency and rate of delivery. Because of this, the studies of interactions between potential anticancer drugs and HSA as a potential drug carrier are of great importance in cancer science. Fluorescence spectroscopy proved to be useful for characterization of small molecule - HSA interactions. Aromatic amino acids Tyr, Phe and Trp can emit light by fluorescence upon excitation with 280 nm light, and among them Trp has the largest quantum yield. The HSA has only one Trp residue (Trp214) which is close to two binding sites where the majority of drug molecules bind (Sudlow site I and II). Upon binding of a small molecule in the vicinity of Trp214 the microenvironment around this residue changes, and this reflects on the emission properties of Trp214.

The changes in emission spectra of HSA with the addition of increasing amount of **1** are shown in Fig. 14. As the concentration of **1** increases, results may deviate from initial linearity due to instrumental inner filter effect [158]. As we used very diluted solutions of HSA and **1**, the absorbances at both excitation and emission wavelength did not exceed 0.05 even for the most concentrated solution, so inner filter effect is negligible and therefore raw spectral data were used for further calculations. The decrease in fluorescence intensity of HSA (fluorescence quenching) is observed, with the slight blue shift of maximum emission at ~340 nm. The change in the maximum emission wavelength indicates that the microenvironment around Trp214 is altered as HSA-**1** complex is formed. After addition of a maximum amount of substance, the final volume of DMSO did not exceed 2%. It was shown that addition of 15% of DMSO does not induce the structural changes in bovine serum albumin, a protein structurally similar to HSA. Therefore, it is unlikely that the conformation of HSA will be changed with the level of DMSO used in this study [159].

Fluorescence quenching data are further processed using Stern-Volmer (S-V) Eq. (1):

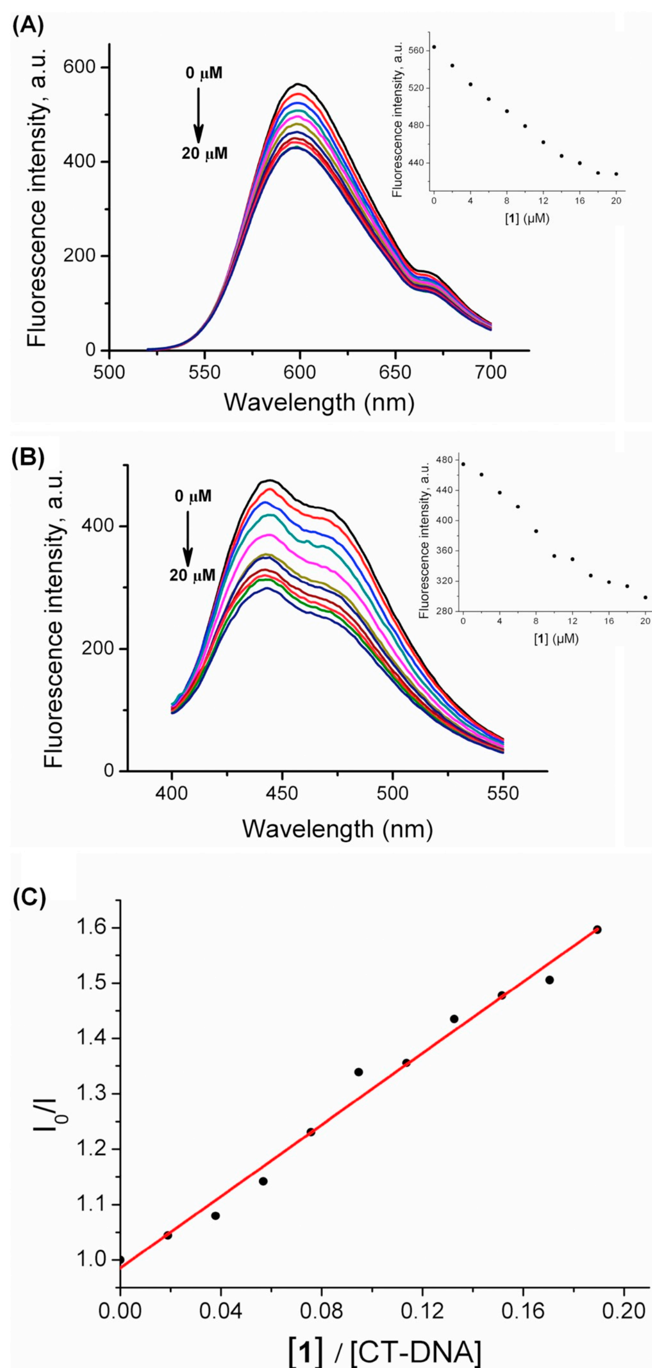

Fig. 12. (A) Emission spectra (λ_{ex} 500 nm) of EB (25 μM) bound to CT-DNA (100 μM, top black line) and quenching of EB–CT-DNA system by **1** at increasing concentrations (0 to 20 μM, curves from top to bottom). The inset demonstrates the saturation of binding. (B) Emission spectra (λ_{ex} 350 nm) of H (28 μM) bound to CT-DNA (100 μM, top black line) and quenching of H–CT-DNA system by **1** at increasing concentrations (0 to 20 μM, curves from top to bottom). The inset demonstrates the saturation of binding. (C) Fluorescence quenching curves of H bound to CT-DNA at λ_{max} 444 nm by **1**.

$$\frac{F_0}{F} = 1 + K_{sv}[Q] = 1 + K_q\tau_0[Q] \tag{1}$$

where F_0 and F represents HSA fluorescence intensities in absence (F_0) and in the presence of the quencher (F); K_{sv} and K_q are S-V's quenching constant and the quenching rate constant of protein, respectively; τ_0 is the average fluorescence lifetime (7.09 ns for HSA [154]), and $[Q]$ is the concentration of the quencher (**1**). The plot $F_0/F = f([Q])$ is shown in Fig. S17 (Supplementary material). Up to 4 equivalents of quencher, S-V's plot is linear with an intercept equal to 1 and slope 5.08×10^4, which is the value for binding constant for **1**. At higher quencher concentrations, the plot deviates from linearity as Trp214 residue become less available to the new molecules of the quencher. Once a bulky molecule of **1** is bound to HSA it makes an approach and binding of a new quencher molecule more difficult.

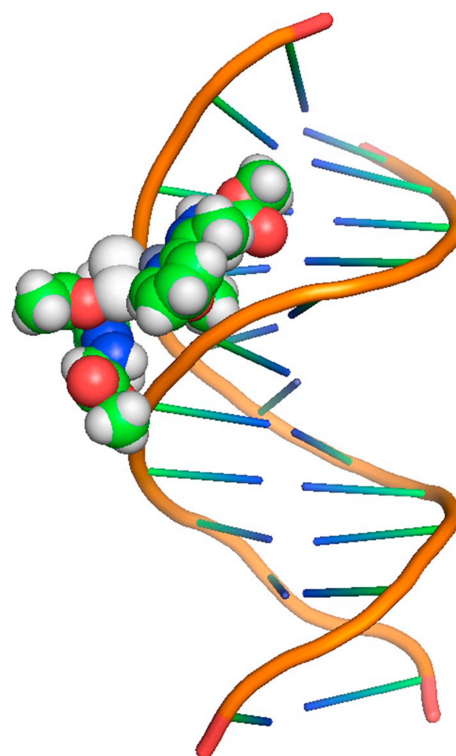

Fig. 13. The most favorable docking solution for **1**-DNA interaction.

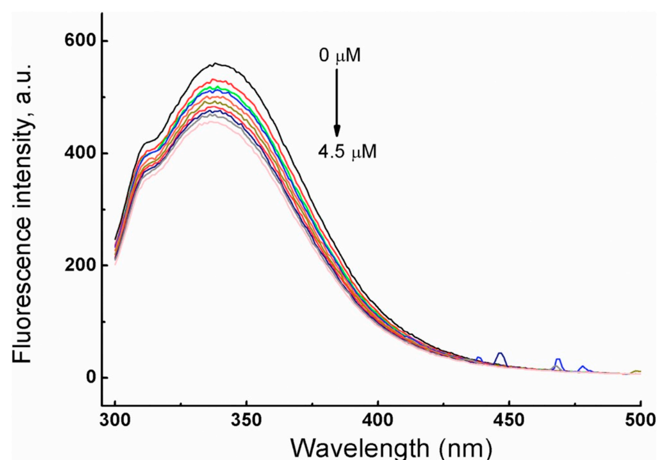

Fig. 14. Changes in fluorescence emission spectrum of HSA ($c = 5.0 \times 10^{-7}$ M, top black line) upon addition of **1** in the concentration range from 0 to 4.5×10^{-6} M; $t = 25$ °C, pH = 7.35.

To evaluate the fractional accessibility of Trp214 residues, we analyzed the quenching data using modified S-V Eq. (1) [160]:

$$\frac{F_0}{\Delta F} = \frac{1}{f_a K_a}\frac{1}{[Q]} + \frac{1}{f_a} \tag{2}$$

where ΔF is the difference in fluorescence intensity of HSA in the absence (F_0) and in the presence of the quencher at concentration $[Q]$. K_a represents the effective quenching constant for the accessible

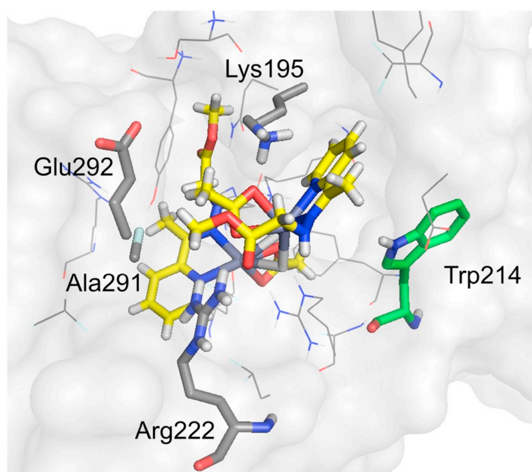

Fig. 15. Complex **1** (carbon atoms shown as yellow sticks) docked into IIA binding site of HSA. Trp214 is shown as green. The amino acid residues that interact with **1** are shown as thick grey sticks.

fluorophores, and f_a is the fraction of the accessible fluorophore. The results of linear fit are shown in Fig. S18 (Supplementary material). Extrapolation to high concentrations of **1** shows that only 25% of total fluorescence intensity of Trp214 was quenched by **1**. As **1** is very bulky compound, it most probably binds simultaneously in the vicinity of Trp214 as well as at the surface of HSA, so only a fraction of a total number of molecules quenches Trp214 emission. Complex **1** binds to HSA with moderate affinity ($K_{sv} = 5.08 \times 10^4\,M^{-1}$), and the affinity of **1** is high enough to be effectively transported and stored by HSA in the body.

*3.7.2. Molecular docking of **1** with HSA*

The docking scores for binding of **1** to three sites of HSA are shown in Table S2 (Supplementary material). Docking scores are very similar for all three binding sites. Complex **1** binds to the site IIA with slight preference. The majority of docking solutions places **1** at the surface of HSA. The large portion of bound molecule is exposed to the solvent, and this may explain relatively weak binding constant found for **1**. Binding mode of **1** to the binding site IIA is shown in Fig. 15. The acetate ligand of **1** interacts with Lys195 and Arg222 through hydrogen bonding (at distances 2.84 and 3.11 Å, respectively). It also interacts with Ala291 and Glu292 through non-specific, hydrophobic contacts. Complex **1** is located far from Trp214 (distance is 4.7 Å) and does not interact with this residue. The fluorescence quenching observed is probably due to the conformational changes in the surroundings of Trp214, induced by the binding of **1**. The moderate binding constant of **1** to HSA is in line with the binding mode found through the molecular docking, as there is a small number of interactions that could stabilize HSA-**1** aduct. A large portion of the bound molecule is solvent-exposed, and water molecules from the medium can compete for the ligand molecule and destabilize protein-ligand complex.

4. Conclusion

Current results on biological activity reveal that our novel binuclear, hydrazone-based cadmium complex **1** is a very strong pro-apoptotic inducer in both, MCF-7 and AsPC-1 cells, even more powerful than CDDP, particularly for AsPC-1 CSCs. While changes in cell cycle distribution signify that **1** interferes in the process of DNA replication, comparative analysis indicates that its mechanism of action differs from the one of CDDP. That hypothesis is confirmed in DNA interaction study where results show non-covalent low binding strength of **1** into DNA minor groove together with the lack of DNA cleavage in pUC19 experiment, which indicates that its target is rather related to protein(s) involved in the control of replication than DNA itself. Furthermore, apoptotic death caused by **1** was maintained mostly in caspase-independent manner and included activation of intrinsic apoptotic cascade, which was quite the opposite of CDDP. The underlying cause for suppressed activation of caspase-8, accompanied with significant inhibition of cross-talk between intrinsic and extrinsic caspase pathways in both cell lines treated with **1**, remains to be further investigated. Although **1** has proved to be a powerful inducer of mitochondrial $O_2\cdot^-$, it still remains unclear whether this mechanism could have an important role in apoptosis induction. Finally, results on 3D spheroids displayed substantial activity of **1** against CSCs. All these results make **1** as a serious candidate for further investigations on other CSC models and as a putative treatment of *e.g.* highly resistant pancreatic cancer.

Abbreviations

CDDP	cisplatin
haOEt × HCl	ethyl hydrazinoacetate hydrochloride
2-ap	2-acetylpyridine
MCF-7	human mammary adenocarcinoma cell line
CSC	cancer stem cell
AsPC-1	human pancreatic adenocarcinoma cell line
2D	two-dimensional
3D	three-dimensional
ATR	Attenuated Total Reflection
RCF	relative centrifugal force
FBS	fetal bovine serum
RPMI	Roswell Park Memorial Institute
DMEM	Dulbecco's modified Eagle's medium
PI	propidium iodide
Annexin V	Ca^{2+}-dependent phospholipid-binding protein with high affinity for phosphatidylserine
Z-VAD-fmk	carbobenzoxy-valyl-alanyl-aspartyl-[*O*-methyl]-fluor-ketone
HSA	human serum albumin
ROS	reactive oxygen species
$O_2\cdot^-$	superoxide anion radical
SOD	superoxide dismutase
MFI	median fluorescent intensity
mPTP	mitochondrial permeability transition pore
MTP	mitochondrial transmembrane potential
7-AAD	7-Aminoactinomycin D
EB	ethidium bromide
H	Hoechst 33258 dye
CT	calf thymus
S-V	Stern-Volmer (equation)

Acknowledgements

The Ministry of Education, Science and Technological Development of the Republic of Serbia under Grant 172055 supported this work.

Appendix A. Supplementary data

Supplementary data to this article can be found online at https://doi.org/10.1016/j.jinorgbio.2018.10.002.

References

[1] B. Kumar, S. Singh, I.-I. Skvortsova, V. Kumar, Promising targets in anti-cancer drug development: recent updates, Curr. Med. Chem. 24 (2017) 1, https://doi.org/10.2174/0929867324666170331123648.

[2] T. Helleday, E. Petermann, C. Lundin, B. Hodgson, R.A. Sharma, DNA repair pathways as targets for cancer therapy, Nat. Rev. Cancer 8 (2008) 193–204, https://doi.org/10.1038/nrc2342.

[3] E. Jamieson, S. Lippard, Structure, recognition, and processing of cisplatin-DNA adducts, Chem. Rev. 99 (1999) 2467–2498, https://doi.org/10.1021/cr980421n.

[4] C.X. Zhang, S.J. Lippard, New metal complexes as potential therapeutics, Curr. Opin. Chem. Biol. 7 (2003) 481–489, https://doi.org/10.1016/S1367-5931(03)00081-4.
[5] T.C. Johnstone, K. Suntharalingam, S.J. Lippard, The next generation of platinum drugs: targeted Pt(II) agents, nanoparticle delivery, and Pt(IV) prodrugs, Chem. Rev. 116 (2016) 3436–3486, https://doi.org/10.1021/acs.chemrev.5b00597.
[6] B. Rosenberg, L. Vancamp, J.E. Trosko, V.H. Mansour, Platinum compounds: a new class of potent antitumour agents, Nature 222 (1969) 385–386, https://doi.org/10.1038/222385a0.
[7] K.D. Mjos, C. Orvig, Metallodrugs in medicinal inorganic chemistry, Chem. Rev. 114 (2014) 4540–4563, https://doi.org/10.1021/cr400460s.
[8] D.M. Cheff, M.D. Hall, A drug of such damned nature.1 challenges and opportunities in translational platinum drug research, J. Med. Chem. 60 (2017) 4517–4532, https://doi.org/10.1021/acs.jmedchem.6b01351.
[9] N.P.E. Barry, P.J. Sadler, Exploration of the medical periodic table: towards new targets, Chem. Commun. 49 (2013) 5106–5131, https://doi.org/10.1039/c3cc41143e.
[10] L.S. Foteeva, M. Matczuk, A.R. Timerbaev, Analytical methodology for determination of interactions between metallodrugs and DNA: a critical examination, TrAC Trends Anal. Chem. 90 (2017) 107–113, https://doi.org/10.1016/j.trac.2017.03.003.
[11] M. Marloye, G. Berger, M. Gelbcke, F. Dufrasne, A survey of the mechanisms of action of anticancer transition metal complexes, Future Med. Chem. 8 (2016) 2263–2286, https://doi.org/10.4155/fmc-2016-0153.
[12] A. de Almeida, B.L. Oliveira, J.D.G. Correia, G. Soveral, A. Casini, Emerging protein targets for metal-based pharmaceutical agents: an update, Coord. Chem. Rev. 257 (2013) 2689–2704, https://doi.org/10.1016/J.CCR.2013.01.031.
[13] K.J. Kilpin, P.J. Dyson, Enzyme inhibition by metal complexes: concepts, strategies and applications, Chem. Sci. 4 (2013) 1410–1419, https://doi.org/10.1039/c3sc22349c.
[14] C.M. Che, F.M. Siu, Metal complexes in medicine with a focus on enzyme inhibition, Curr. Opin. Chem. Biol. 14 (2010) 255–261, https://doi.org/10.1016/j.cbpa.2009.11.015.
[15] L.H. Swift, R.M. Golsteyn, Genotoxic anti-cancer agents and their relationship to DNA damage, mitosis, and checkpoint adaptation in proliferating cancer cells, Int. J. Mol. Sci. 15 (2014) 3403–3431, https://doi.org/10.3390/ijms15033403.
[16] Y.X. Tai, Y.M. Ji, Y.L. Lu, M.X. Li, Y.Y. Wu, Q.X. Han, Cadmium(II) and indium(III) complexes derived from 2-benzoylpyridine *N*(4)-cyclohexylthiosemicarbazone: synthesis, crystal structures, spectroscopic characterization and cytotoxicity, Synth. Met. 219 (2016) 109–114, https://doi.org/10.1016/j.synthmet.2016.05.015.
[17] Z. Zhang, C. Bi, D. Buac, Y. Fan, X. Zhang, J. Zuo, P. Zhang, N. Zhang, L. Dong, Q.P. Dou, Organic cadmium complexes as proteasome inhibitors and apoptosis inducers in human breast cancer cells, J. Inorg. Biochem. 123 (2013) 1–10, https://doi.org/10.1016/j.jinorgbio.2013.02.004.
[18] D. Solaiman, L.A. Saryan, D.H. Petering, Reactions of 3-ethoxy-2-oxobutyraldehyde bis(N^4-dimethylthiosemicarbazonato) cadmium with tumor cells, J. Inorg. Biochem. 10 (1979) 135–146, https://doi.org/10.1016/S0162-0134(00)81013-2.
[19] M.T.H. Tarafder, A.M. Ali, M.S. Elias, K.A. Crouse, S. Silong, Coordination chemistry and biological activity of bidentate and quadridentate nitrogen ± sulfur donor ligands and their complexes, Transit. Met. Chem. 25 (2000) 706–710, https://doi.org/10.1023/A:1007069601569.
[20] R. Manikandan, N. Chitrapriya, Y.J. Jang, P. Viswanathamurthi, Evaluation of DNA-binding, radical scavenging and cytotoxic activity of five coordinated Cd(II) complexes containing 2-acetylpyridine-N_4-substituted thiosemicarbazone, RSC Adv. 3 (2013) 11647, https://doi.org/10.1039/c3ra40814k.
[21] O.A. El-Gammal, G.M. Abu El-Reash, M.M. El-Gamil, Structural, spectral, pH-metric and biological studies on mercury (II), cadmium (II) and binuclear zinc (II) complexes of NS donor thiosemicarbazide ligand, Spectrochim. Acta A 123 (2014) 59–70, https://doi.org/10.1016/j.saa.2013.12.034.
[22] J.M. Pérez, A.I. Matesanz, A. Martín-Ambite, P. Navarro, C. Alonso, P. Souza, Synthesis and characterization of complexes of *p*-isopropyl benzaldehyde and methyl 2-pyridyl ketone thiosemicarbazones with Zn(II) and Cd(II) metallic centers. Cytotoxic activity and induction of apoptosis in Pam-ras cells, J. Inorg. Biochem. 75 (1999) 255–261, https://doi.org/10.1016/S0162-0134(99)00096-3.
[23] I.H. Hall, C.B. Lackey, T.D. Kistler, J.S. Ives, H. Beraldo, L.J. Ackerman, D.X. West, The cytotoxicity of symmetrical and unsymmetrical bis(thiosemicarbazones) and their metal complexes in murine and human tumor cells, Arch. Pharm. 333 (2000) 217–225, https://doi.org/10.1002/1521-4184(20007)333:7<217::AID-ARDP217>3.0.CO;2-M.
[24] D. Zhang, Q. Li, M.X. Li, D.Y. Chen, J.Y. Niu, Cytotoxic activity of iron(III), cobalt (III), nickel(II), zinc(II), and cadmium(II) complexes of 2-acetylpyrazine thiosemicarbazone: crystal structure of the cobalt(III) complex, J. Coord. Chem. 63 (2010) 1063–1070, https://doi.org/10.1080/00958971003706706.
[25] S. Bjelogrlic, T. Todorovic, A. Bacchi, M. Zec, D. Sladic, T. Srdic-Rajic, D. Radanovic, S. Radulovic, G. Pelizzi, K. Andelkovic, Synthesis, structure and characterization of novel Cd(II) and Zn(II) complexes with the condensation product of 2-formylpyridine and selenosemicarbazide. Antiproliferative activity of the synthesized complexes and related selenosemicarbazone complexes, J. Inorg. Biochem. 104 (2010) 673–682, https://doi.org/10.1016/j.jinorgbio.2010.02.009.
[26] M. Zec, T. Srdic-Rajic, A. Konic-Ristic, T. Todorovic, K. Andjelkovic, I. Filipovic-Ljeskovic, S. Radulovic, Anti-metastatic and anti-angiogenic properties of potential new anti-cancer drugs based on metal complexes of selenosemicarbazones, Anti Cancer Agents Med. Chem. 12 (2012) 1071–1080, https://doi.org/10.2174/187152012803529682.
[27] N. Gligorijević, T. Todorović, S. Radulović, D. Sladić, N. Filipović, D. Gođevac, D. Jeremić, K. Anđelković, Synthesis and characterization of new Pt(II) and Pd(II) complexes with 2-quinolinecarboxaldehyde selenosemicarbazone: cytotoxic activity evaluation of Cd(II), Zn(II), Ni(II), Pt(II) and Pd(II) complexes with heteroaromatic selenosemicarbazones, Eur. J. Med. Chem. 44 (2009) 1623–1629, https://doi.org/10.1016/j.ejmech.2008.07.033.
[28] O.A. El-Gammal, G.M. Abu El-Reash, S.E. Ghazy, A.H. Radwan, Synthesis, characterization, molecular modeling and antioxidant activity of (1*E*,5*E*)-1,5-bis (1-(pyridin-2-yl)ethylidene)carbonohydrazide (H_2APC) and its zinc(II), cadmium (II) and mercury(II) complexes, J. Mol. Struct. 1020 (2012) 6–15, https://doi.org/10.1016/j.molstruc.2012.04.029.
[29] T.A. Yousef, G.M. Abu El-Reash, M. Al-Jahdali, E.B.R. El-Rakhawy, Synthesis, spectral characterization and biological evaluation of Mn(II), Co(II), Ni(II), Cu(II), Zn(II) and Cd(II) complexes with thiosemicarbazone ending by pyrazole and pyridyl rings, Spectrochim. Acta A 129 (2014) 163–172, https://doi.org/10.1016/j.saa.2014.02.184.
[30] J.M. Pérez, V. Cerrillo, A.I. Matesanz, J.M. Millán, P. Navarro, C. Alonso, P. Souza, DNA interstrand cross-linking efficiency and cytotoxic activity of novel cadmium (II)-thiocarbodiazone complexes, ChemBioChem 2 (2001) 119–123, https://doi.org/10.1002/1439-7633(20010202)2:2<119::AID-CBIC119>3.0.CO;2-5.
[31] N.A. Illán-Cabeza, R.A. Vilaplana, Y. Alvarez, K. Akdi, S. Kamah, F. Hueso-Ureña, M. Quirós, F. González-Vílchez, M.N. Moreno-Carretero, Synthesis, structure and biological activity of a new and efficient Cd(II)-uracil derivative complex system for cleavage of DNA, J. Biol. Inorg. Chem. 10 (2005) 924–934, https://doi.org/10.1007/s00775-005-0045-x.
[32] N.A. Illán-Cabeza, S.B. Jiménez-Pulido, J.M. Martínez-Martos, M.J. Ramírez-Expósito, M.N. Moreno-Carretero, New 2,6-bis-[uracil-imino] ethylpyridine complexes containing the CdN6 core: synthesis, crystal structures, luminescent properties and antiproliferative activity against C6 glioma cells, J. Inorg. Biochem. 103 (2009) 1176–1184, https://doi.org/10.1016/j.jinorgbio.2009.06.007.
[33] Q.Y. Huang, Z.B. Zheng, Y.P. Diao, Synthesis, characterization and anticancer activity of a Cd(II) complex with in situ formation of (*E*)-1-(5-chloro-2-hydroxy-benzylideneamino)-pyrrolidin-2-one ligand, J. Mol. Struct. 1088 (2015) 118–122, https://doi.org/10.1016/j.molstruc.2015.02.022.
[34] N. Zhang, Y. Fan, G. Huang, D. Buac, C. Bi, Y. Ma, X. Wang, Z. Zhang, X. Zhang, Q.P. Dou, L-Tryptophan Schiff base cadmium(II) complexes as a new class of proteasome inhibitors and apoptosis inducers in human breast cancer cells, Inorg. Chim. Acta 466 (2017) 478–485, https://doi.org/10.1016/j.ica.2017.07.006.
[35] N. Zhang, Y.H. Fan, Z. Zhang, J. Zuo, P.F. Zhang, Q. Wang, S. Bin Liu, C.F. Bi, Syntheses, crystal structures and anticancer activities of three novel transition metal complexes with Schiff base derived from 2-acetylpyridine and L-tryptophan, Inorg. Chem. Commun. 22 (2012) 68–72, https://doi.org/10.1016/j.inoche.2012.05.022.
[36] M. Ravi, K.P. Chennam, B. Ushaiah, R.K. Eslavath, S. Perugu, R. Ajumeera, C.S. Devi, A study on spectro-analytical aspects, DNA-interaction, photo-cleavage, radical scavenging, cytotoxic activities, antibacterial and docking properties of 3-(1-(6-methoxybenzo[*d*]thiazol-2-ylimino) ethyl)-6-methyl-3*H*-pyran-2,4-dio, J. Fluoresc. 25 (2015) 1279–1296, https://doi.org/10.1007/s10895-015-1616-z.
[37] N.R. Filipović, A. Bacchi, M. Lazić, G. Pelizzi, S. Radulović, D.M. Sladić, T.R. Todorović, K.K. Anđelković, Synthesis, structure and cytotoxic activity evaluation of a dinuclear complex of Cd(II) with *N'*,*N'*2-bis[(1*E*)-1-(2-pyridyl)ethylidene]propanedihydrazide, Inorg. Chem. Commun. 11 (2008) 47–50, https://doi.org/10.1016/j.inoche.2007.10.013.
[38] H.-Y. Luo, J.-Y. Li, Y. Li, L. Zhang, J.-Y. Li, D.-Z. Jia, G.-C. Xu, Cadmium(II) complexes with a 4-acyl pyrazolone derivative and co-ligands: crystal structures and antitumor activity, RSC Adv. 6 (2016) 114997–115009, https://doi.org/10.1039/C6RA23938B.
[39] T.A. Yousef, S.F. Ahmed, O.A. El-Gammal, G.M. Abu El-Reash, Structural, spectral, thermal and biological studies on (*Z*)-*N*-benzoyl-*N'*-(2-oxo-2-(phenylamino)acetyl) carbamohydrazonothioic acid (H_2PABT) and its Cd(II), Hg(II), Zn(II) and U(VI) O_2^{2+} complexes, Spectrochim. Acta A 146 (2015) 228–239, https://doi.org/10.1016/j.saa.2015.01.128.
[40] S.A. Al-Harbi, M.S. Bashandy, H.M. Al-Saidi, A.A.A. Emara, T.A.A. Mousa, Synthesis, spectroscopic properties, molecular docking, anti-colon cancer and antimicrobial studies of some novel metal complexes for 2-amino-4-phenylthiazole derivative, Spectrochim. Acta A 145 (2015) 425–439, https://doi.org/10.1016/j.saa.2015.03.054.
[41] N.K. Kaushik, A. Mishra, A. Ali, J.S. Adhikari, A.K. Verma, R. Gupta, Synthesis, characterization, and antibacterial and anticancer screening of {M^{2+}-Co^{3+}-M^{2+}} and {Co^{3+}-M^{2+}} (M is Zn, Cd, Hg) heterometallic complexes, J. Biol. Inorg. Chem. 17 (2012) 1217–1230, https://doi.org/10.1007/s00775-012-0937-5.
[42] Y.M. Ji, Y. Fang, P.P. Han, M.X. Li, Q.Q. Chen, Q.X. Han, Copper(II) and cadmium (II) complexes derived from Strandberg-type polyoxometalate clusters: synthesis, crystal structures, spectroscopy and biological activities, Inorg. Chem. Commun. 86 (2017) 22–25, https://doi.org/10.1016/j.inoche.2017.09.014.
[43] A. Chidambaram, A. Sekar, KSH, R.K. Chidambaram, K. Arunachalam, SGP, R. Vilwanathan, Synthesis, characterization, and evaluation of Cd[L-proline]$_2$, a novel histone deacetylase inhibitor that induces epigenetic modification of histone deacetylase isoforms in A549 cells, Investig. New Drugs 35 (2017) 691–705, https://doi.org/10.1007/s10637-017-0489-1.
[44] X. Lv, C. Bi, Y. Fan, X. Zhang, N. Zhang, P. Zhang, Synthesis, characterization and antitumor activity of novel cadmium complex with laminine ligand, Asian J. Chem. 27 (2015) 224–228, https://doi.org/10.14233/ajchem.2015.16879.
[45] Y. Yang, C.-G. Li, X.-J. Luo, Z.-H. Luo, R.-J. Liu, Y.-X. Jiang, W.-J. Liang, Synthesis, crystal structure and DNA interaction studies of a 2D cadmium(II) coordination polymer constructed from 2-(2-pyridyl)benzimidazole, Supramol. Chem. 27

(2015) 281–286, https://doi.org/10.1080/10610278.2014.959015.
[46] C. Hopa, H. Yildirim, H. Kara, R. Kurtaran, M. Alkan, Synthesis, characterization and anti-proliferative activity of Cd(II) complexes with NNN type pyrazole-based ligand and pseudohalide ligands as coligand, Spectrochim. Acta A 121 (2014) 282–287, https://doi.org/10.1016/j.saa.2013.10.028.
[47] M. Umadevi, A. Ramu, V. Muthuraj, P. Saravana, Spectral investigation, structural assignments and anti-tumor activities of pyrimidine based transition metal (II) complexes, Am. J. PharmTech Res. 3 (2013) 415–429.
[48] Q.-L. Guan, Z. Liu, W.-J. Wei, Y.-H. Xing, J. Liu, R. Zhang, Y.-N. Hou, X. Wang, F.-Y. Bai, Synthesis, structure, spectroscopy of four novel supramolecular complexes and cytotoxicity study by application of multiple parallel perfused microbioreactors, New J. Chem. 38 (2014) 3258–3268, https://doi.org/10.1039/C3NJ01646C.
[49] J. Zhao, K. Peng, Y. Guo, J. Zhang, S. Chen, J. Hu, Photoluminescent and cytotoxic properties of multinuclear complexes and multinuclear-based polymers with group 12 metals and a tripodal ligand, New J. Chem. 39 (2015) 6016–6024, https://doi.org/10.1039/C5NJ00222B.
[50] T. Karmakar, Y. Kuang, N. Neamati, J.B. Baruah, Cadmium complexes and cocrystals of indium complexes of benzothiazole derivatives and anticancer activities of the cadmium complexes, Polyhedron 54 (2013) 285–293, https://doi.org/10.1016/j.poly.2013.02.068.
[51] B. Barszcz, J. Masternak, M. Hodorowicz, E. Matczak-Jon, A. Jabłońska-Wawrzycka, K. Stadnicka, M. Zienkiewicz, K. Królewska, J. Kaźmierczak-Barańska, Synthesis, crystal structure and NMR investigation of novel Ca(II) complexes with heterocyclic alcohol, aldehyde and carboxylate ligands. Evaluation of Ca(II) and Cd(II) analogues for anticancer activity, Inorg. Chim. Acta 399 (2013) 85–94, https://doi.org/10.1016/j.ica.2013.01.004.
[52] M. Shebl, Coordination behavior of new bis(tridentate ONO, ONS and ONN) donor hydrazones towards some transition metal ions: synthesis, spectral, thermal, antimicrobial and antitumor studies, J. Mol. Struct. 1128 (2017) 79–93, https://doi.org/10.1016/j.molstruc.2016.08.056.
[53] S.A. Shaker, H. Khaledi, S.C. Cheah, H.M. Ali, New Mn(II), Ni(II), Cd(II), Pb(II) complexes with 2-methylbenzimidazole and other ligands. Synthesis, spectroscopic characterization, crystal structure, magnetic susceptibility and biological activity studies, Arab. J. Chem. 9 (2016) S1943–S1950, https://doi.org/10.1016/j.arabjc.2012.06.013.
[54] C. Ma, S.-K. Liang, F.-C. Zhao, Y. Meng, Y.-Y. Li, M.-C. Zhu, E.-J. Gao, Cadmium(II) complex with 2-methyl-1*H*-4,5-imidazoledicarboxylic acid ligand: synthesis, characterization, and biological activity, J. Coord. Chem. 67 (2014) 3551–3564, https://doi.org/10.1080/00958972.2014.970540.
[55] G. Cristalli, P. Franchetti, E. Nasini, S. Vittori, M. Grifantini, A. Barzi, E. Lepri, S. Ripa, Metal(II)complexes of 2,2′-bipyridyl-6-carbothioamide anti-tumor and anti-fungal agents, Eur. J. Med. Chem. 23 (1988) 301–305, https://doi.org/10.1016/0223-5234(88)90014-1.
[56] X. Chen, J. Wu, Q. Yang, X. Zhang, P. Zhang, S. Liao, Z. He, X. Wang, C. Zhao, J. Liu, Cadmium pyrithione suppresses tumor growth in vitro and in vivo through inhibition of proteasomal deubiquitinase, BioMetals 31 (2018) 29–43, https://doi.org/10.1007/s10534-017-0062-6.
[57] R. Chen, C. Sen Liu, H. Zhang, Y. Guo, X.H. Bu, M. Yang, Three new Cu(II) and Cd (II) complexes with 3-(2-pyridyl)pyrazole-based ligand: syntheses, crystal structures, and evaluations for bioactivities, J. Inorg. Biochem. 101 (2007) 412–421, https://doi.org/10.1016/j.jinorgbio.2006.11.001.
[58] A. Kareem, H. Zafar, A. Sherwani, O. Mohammad, T.A. Khan, Synthesis, characterization and in vitro anticancer activity of 18-membered octaazamacrocyclic complexes of Co(II), Ni(II), Cd(II) and Sn(II), J. Mol. Struct. 1075 (2014) 17–25, https://doi.org/10.1016/j.molstruc.2014.06.073.
[59] X. Zhou, Y. Koizumi, M. Zhang, M. Natsui, S. Koyota, M. Yamada, Y. Kondo, F. Hamada, T. Sugiyama, Cadmium-coordinated supramolecule suppresses tumor growth of T-cell leukemia in mice, Cancer Sci. 106 (2015) 635–641, https://doi.org/10.1111/cas.12651.
[60] F. Zhang, X.L. Zheng, Q.Y. Lin, P.P. Wang, W.J. Song, Two novel cadmium(II) complexes with demethylcantharate and polypyridyl: crystal structure, interactions with DNA and bovine serum albumin, Inorg. Chim. Acta 394 (2013) 85–91, https://doi.org/10.1016/j.ica.2012.07.030.
[61] L. Tabrizi, H. Chiniforoshan, P. McArdle, Synthesis, crystal structure and spectroscopy of bioactive Cd(II) polymeric complex of the non-steroidal anti-inflammatory drug diclofenac sodium: antiproliferative and biological activity, Spectrochim. Acta A 136 (2015) 429–436, https://doi.org/10.1016/j.saa.2014.09.053.
[62] D. Kovala-Demertzi, M. Staninska, I. Garcia-Santos, A. Castineiras, M.A. Demertzis, Synthesis, crystal structures and spectroscopy of meclofenamic acid and its metal complexes with manganese(II), copper(II), zinc(II) and cadmium (II). Antiproliferative and superoxide dismutase activity, J. Inorg. Biochem. 105 (2011) 1187–1195, https://doi.org/10.1016/j.jinorgbio.2011.05.025.
[63] N.S. Rukk, L.G. Kuzmina, D.V. Albov, R.S. Shamsiev, S.N. Mudretsova, G.A. Davydova, V.M. Retivov, P.A. Volkov, V.V. Kravchenko, G.N. Apryshko, A.N. Streletskii, A.Y. Skryabina, E.A. Mironova, V.V. Zamalyutin, Synthesis, X-ray crystal structure and cytotoxicity studies of zinc(II) and cadmium(II) iodide complexes with antipyrine, Polyhedron 102 (2015) 152–162, https://doi.org/10.1016/j.poly.2015.09.011.
[64] L. Tabrizi, R. Golbang, H. Sadeghi, H. Chiniforoshan, P. Mcardle, B. Notash, Dinuclear cadmium indomethacin and Lawsone complexes: synthesis, crystal structures, antiproliferative and biological evaluations, J. Coord. Chem. 69 (2016) 3021–3034, https://doi.org/10.1080/00958972.2016.1223845.
[65] J. Masternak, B. Barszcz, W. Sawka-Dobrowolska, J. Wietrzyk, J. Jezierska, M. Milczarek, An efficient process to directly convert 1-hydroxymethyl-3,5-dimethylpyrazole to Cd(II) complexes via C−N bond creation: cytotoxicity and factors controlling the structures, RSC Adv. 4 (2014) 43962–43972, https://doi.org/10.1039/C4RA07960D.
[66] M.I. Khalil, A.M. Al-Zahem, M.M. Qunaibit, Synthesis, characterization, and antitumor activity of binuclear curcumin-metal(II) hydroxo complexes, Med. Chem. Res. 23 (2014) 1683–1689, https://doi.org/10.1007/s00044-013-0727-9.
[67] K.B. Chew, M.T.H. Tarafder, K.A. Crouse, A.M. Ali, B.M. Yamin, H.K. Fun, Synthesis, characterization and bio-activity of metal complexes of bidentate N-S isomeric Schiff bases derived from *S*-methyldithiocarbazate (SMDTC) and the X-ray structure of the bis[*S*-methyl-β-*N*-(2-furyl-methylketone) dithiocarbazato] cadmium(II) complex, Polyhedron 23 (2004) 1385–1392, https://doi.org/10.1016/j.poly.2004.02.018.
[68] M.T.H. Tarafder, A. Kasbollah, K.A. Crouse, A.M. Ali, B.M. Yamin, H.K. Fun, Synthesis and characterization of Zn(II) and Cd(II) complexes of *S*-benzyl-β-*N*-(2-pyridyl)methylenedithiocarbazate (HNNS): bioactivity of the HNNS Schiff base and its Zn(II), Cu(II) and Cd(II) complexes and the X-ray structure of the [Zn(NNS)$_2$] complex, Polyhedron 20 (2001) 2363–2370, https://doi.org/10.1016/S0277-5387(01)00817-8.
[69] M.T. Tarafder, K.T. Jin, K.A. Crouse, A. Ali, B. Yamin, H.-K. Fun, Coordination chemistry and bioactivity of Ni^{2+}, Cu^{2+}, Cd^{2+} and Zn^{2+} complexes containing bidentate Schiff bases derived from S-benzyldithiocarbazate and the X-ray crystal structure of bis[*S*-benzyl-β-*N*-(5-methyl-2-furylmethylene)dithiocarbazato]cadmium(II), Polyhedron 21 (2002) 2547–2554, https://doi.org/10.1016/S0277-5387(02)01188-9.
[70] T.J. Khoo, M.K. Bin Break, K.A. Crouse, M.I.M. Tahir, A.M. Ali, A.R. Cowley, D.J. Watkin, M.T.H. Tarafder, Synthesis, characterization and biological activity of two Schiff base ligands and their nickel(II), copper(II), zinc(II) and cadmium(II) complexes derived from *S*-4-picolyldithiocarbazate and X-ray crystal structure of cadmium(II) complex derived from pyridine-2-carboxaldehyde, Inorg. Chim. Acta 413 (2014) 68–76, https://doi.org/10.1016/j.ica.2014.01.001.
[71] M.H.E. Chan, K.A. Crouse, M.I.M. Tahir, R. Rosli, N. Umar-Tsafe, A.R. Cowley, Synthesis and characterization of cobalt(II), nickel(II), copper(II), zinc(II) and cadmium(II) complexes of benzyl *N*-[1-(thiophen-2-yl)ethylidene] hydrazine carbodithioate and benzyl *N*-[1-(thiophen-3-yl)ethylidene] hydrazine carbodithioate and the X-ray crystal structure of bis{benzyl *N*-[1-(thiophen-2-yl)ethylidene] hydrazine carbodithioate}nickel(II), Polyhedron 27 (2008) 1141–1149, https://doi.org/10.1016/j.poly.2007.11.035.
[72] D.D. Yang, Y.N. Chen, Y.S. Wu, R. Wang, Z.J. Chen, J. Qin, S.S. Qian, H.L. Zhu, Synthesis, crystal structures, molecular docking, and in vitro biological activities of transition metals with 4-(2,3-dichlorophenyl)piperazine-1-carboxylic acid, Bioorg. Med. Chem. Lett. 26 (2016) 3295–3299, https://doi.org/10.1016/j.bmcl.2016.05.051.
[73] N.R. Filipović, T.R. Todorović, D.M. Sladić, I.T. Novaković, D.A. Jeremić, K.K. Andjelković, Synthesis, characterization and biological activity evaluation of novel Pd(II) and Pt(II) complexes with heterocyclic hydrazone ligands, Mater. Sci. Forum 555 (2007) 423–427, https://doi.org/10.4028/www.scientific.net/MSF.555.423.
[74] N. Filipović, H. Borrmann, T. Todorović, M. Borna, V. Spasojević, D. Sladić, I. Novaković, K. Andjelković, Copper(II) complexes of *N*-heteroaromatic hydrazones: synthesis, X-ray structure, magnetic behavior, and antibacterial activity, Inorg. Chim. Acta 362 (2009) 1996–2000, https://doi.org/10.1016/j.ica.2008.09.019.
[75] N. Filipović, T. Todorović, R. Marković, A. Marinković, S. Tufegdžić, D. Gođevac, K. Anđelković, Synthesis, characterization and biological activities of *N*-heteroaromatic hydrazones and their complexes with Pd(II), Pt(II) and Cd(II), Transit. Met. Chem. 35 (2010) 765–772, https://doi.org/10.1007/s11243-010-9391-9.
[76] N. Filipović, T. Todorović, D. Radanović, V. Divjaković, R. Marković, I. Pajić, K. Anelković, Solid state and solution structures of Cd(II) complexes with two *N*-heteroaromatic Schiff bases containing ester groups, Polyhedron 31 (2012) 19–28, https://doi.org/10.1016/j.poly.2011.07.023.
[77] N.R. Filipović, I. Marković, D. Mitić, N. Polović, M. Milčić, M. Dulović, M. Jovanović, M. Savić, M. Nikšić, K. Anđelković, T. Todorović, A comparative study of in vitro cytotoxic, antioxidant, and antimicrobial activity of Pt(II), Zn(II), Cu(II), and Co(III) complexes with *N*-heteroaromatic Schiff Base (*E*)-2-[*N′*-(1-pyridin-2-yl-ethylidene)hydrazino]acetate, J. Biochem. Mol. Toxicol. 28 (2014) 99–110, https://doi.org/10.1002/jbt.21541.
[78] N. Filipović, S. Grubišić, M. Jovanović, M. Dulović, I. Marković, O. Klisurić, A. Marinković, D. Mitić, K. Anđelković, T. Todorović, Palladium(II) complexes with *N*-heteroaromatic bidentate hydrazone ligands: the effect of the chelate ring size and lipophilicity on *in vitro* cytotoxic activity, Chem. Biol. Drug Des. 84 (2014) 333–341, https://doi.org/10.1111/cbdd.12322.
[79] T. Todorovic, S. Grubišic, M. Pregelj, M. Jagodič, S. Misirlic-Denčic, M. Dulovic, I. Markovic, O. Klisuric, A. Malešević, D. Mitic, K. Anđelković, N. Filipovic, Structural, magnetic, DFT, and biological studies of mononuclear and dinuclear Cu (II) complexes with bidentate *N*-heteroaromatic Schiff base ligands, Eur. J. Inorg. Chem. 2015 (2015) 3921–3931, https://doi.org/10.1002/ejic.201500349.
[80] Ş. Comşa, A.M. Cîmpean, M. Raica, The story of MCF-7 breast cancer cell line: 40 years of experience in research, Anticancer Res. 3154 (2015) 3147–3154.
[81] P.B. Gupta, C.M. Fillmore, G. Jiang, S.D. Shapira, K. Tao, C. Kuperwasser, E.S. Lander, Stochastic state transitions give rise to phenotypic equilibrium in populations of cancer cells, Cell 146 (2011) 633–644, https://doi.org/10.1016/j.cell.2011.07.026.
[82] F.H. Sarkar, Y. Li, Z. Wang, D. Kong, Pancreatic cancer stem cells and EMT in drug resistance and metastasis, Minerva Chir. 64 (2009) 489–500.
[83] T. Arumugam, V. Ramachandran, K.F. Fournier, H. Wang, L. Marquis,

J.L. Abbruzzese, G.E. Gallick, C.D. Logsdon, D.J. McConkey, W. Choi, Epithelial to mesenchymal transition contributes to drug resistance in pancreatic cancer, Cancer Res. 69 (2009) 5820–5828, https://doi.org/10.1158/0008-5472.CAN-08-2819.

[84] B. Beck, C. Blanpain, Unravelling cancer stem cell potential, Nat. Rev. Cancer 13 (2013) 727–738, https://doi.org/10.1038/nrc3597.

[85] P.A. Sotiropoulou, M.S. Christodoulou, A. Silvani, C. Herold-Mende, D. Passarella, Chemical approaches to targeting drug resistance in cancer stem cells, Drug Discov. Today 19 (2014) 1547–1562, https://doi.org/10.1016/J.DRUDIS.2014.05.002.

[86] M.S. Sosa, P. Bragado, J.A. Aguirre-Ghiso, Mechanisms of disseminated cancer cell dormancy: an awakening field, Nat. Rev. Cancer 14 (2014) 611–622, https://doi.org/10.1038/nrc3793.

[87] J.W. Uhr, K. Pantel, Controversies in clinical cancer dormancy, Proc. Natl. Acad. Sci. 108 (2011) 12396–12400, https://doi.org/10.1073/pnas.1106613108.

[88] R.P. Galvao, A. Kasina, R.S. McNeill, J.E. Harbin, O. Foreman, R.G.W. Verhaak, A. Nishiyama, C.R. Miller, H. Zong, Transformation of quiescent adult oligodendrocyte precursor cells into malignant glioma through a multistep reactivation process, Proc. Natl. Acad. Sci. 111 (2014) E4214–E4223, https://doi.org/10.1073/pnas.1414389111.

[89] M. Zanoni, F. Piccinini, C. Arienti, A. Zamagni, S. Santi, R. Polico, A. Bevilacqua, A. Tesei, 3D tumor spheroid models for in vitro therapeutic screening: a systematic approach to enhance the biological relevance of data obtained, Sci. Rep. 6 (2016) 19103, , https://doi.org/10.1038/srep19103.

[90] Agilent Technologies UK Ltd, CrysAlisPro Software System, (2014).

[91] G.M. Sheldrick, *SHELXT* – integrated space-group and crystal-structure determination, Acta Crystallogr. A Found. Adv. 71 (2015) 3–8, https://doi.org/10.1107/S2053273314026370.

[92] G.M. Sheldrick, Crystal structure refinement with *SHELXL*, Acta Crystallogr. C 71 (2015) 3–8, https://doi.org/10.1107/S2053229614024218.

[93] C.B. Hübschle, G.M. Sheldrick, B. Dittrich, *ShelXle*: a Qt graphical user interface for *SHELXL*, J. Appl. Crystallogr. 44 (2011) 1281–1284, https://doi.org/10.1107/S0021889811043202.

[94] A.L. Spek, Structure validation in chemical crystallography, Acta Crystallogr. D65 (2009) 148–155, https://doi.org/10.1107/S090744490804362X.

[95] J. van de Streek, P.A. Wood, C.F. Macrae, I.J. Bruno, J.A. Chisholm, P.R. Edgington, P. McCabe, E. Pidcock, L. Rodriguez-Monge, R. Taylor, Mercury CSD 2.0 - new features for the visualization and investigation of crystal structures, J. Appl. Crystallogr. 41 (2008) 466–470, https://doi.org/10.1107/S0021889807067908.

[96] C.R. Groom, I.J. Bruno, M.P. Lightfoot, S.C. Ward, The Cambridge structural database, Acta Crystallogr. B 72 (2016) 171–179, https://doi.org/10.1107/S2052520616003954.

[97] C.F. Mackenzie, P.R. Spackman, D. Jayatilaka, M.A. Spackman, CrystalExplorer model energies and energy frameworks: extension to metal coordination compounds, organic salts, solvates and open-shell systems, IUCrJ 4 (2017) 575–585, https://doi.org/10.1107/S205225251700848X.

[98] M.J. Turner, J.J. McKinnon, S.K. Wolff, D.J. Grimwood, P.R. Spackman, D. Jayatilaka, M.A. Spackman, CrystalExplorer17, University of Western Australia, 2017.

[99] M.A. Spackman, P.G. Byrom, A novel definition of a molecule in a crystal, Chem. Phys. Lett. 267 (1997) 215–220, https://doi.org/10.1016/S0009-2614(97)00100-0.

[100] N.R. Filipović, A. Bacchi, G. Pelizzi, R. Marković, D. Mitić, K.K. Anđelković, Cobalt (III), zinc(II), cadmium(II) and palladium(II) complexes with the hydrolysed and non-hydrolysed condensation products of 2-acetylpyridine with ethyl hydrazinoacetate: X-ray structure analysis of *mer*-bis{(*E*)-2-[*N*′-(1-pyridin-2-yl-ethylidene)hydrazinino] acetato}cobalt(III) tetrafluoroborate, J. Coord. Chem. 58 (2005) 1541–1550, https://doi.org/10.1080/00958970500240383.

[101] N. Filipović, M. Borna, O. Klisurić, M. Pregelj, M. Jagodič, K. Anđelković, T. Todorović, Synthesis, characterization, and thermal behavior of Cu(II) and Zn (II) complexes with (*E*)-2-[N′-(1-pyridin-2-yl-ethylidene)hydrazino]acetic acid (aphaOH). Crystal structure of $[Zn_2(aphaO)_2Cl_2]$, J. Coord. Chem. 66 (2013) 1549–1560, https://doi.org/10.1080/00958972.2013.786052.

[102] K. Nakamoto, Infrared and Raman Spectra of Inorganic and Coordination Compounds, John Wiley & Sons, Inc., Hoboken, NJ, USA, 2008, https://doi.org/10.1002/9780470405840.

[103] W.J. Geary, The use of conductivity measurements in organic solvents for the characterisation of coordination compounds, Coord. Chem. Rev. 7 (1971) 81–122, https://doi.org/10.1016/S0010-8545(00)80009-0.

[104] C. Janiak, A critical account on π–π stacking in metal complexes with aromatic nitrogen-containing ligands, Dalton Trans. (2000) 3885–3896, https://doi.org/10.1039/b003010o.

[105] A. Gavezzotti, The "sceptical chymist": intermolecular doubts and paradoxes, CrystEngComm 15 (2013) 4027, https://doi.org/10.1039/c3ce00051f.

[106] M.J. Turner, S.P. Thomas, M.W. Shi, D. Jayatilaka, M.A. Spackman, Energy frameworks: insights into interaction anisotropy and the mechanical properties of molecular crystals, Chem. Commun. 51 (2015) 3735–3738, https://doi.org/10.1039/C4CC09074H.

[107] B. Čobeljić, A. Pevec, S. Stepanović, M.R. Milenković, I. Turel, M. Gruden, D. Radanović, K. Anđelković, Structural diversity of isothiocyanato Cd(II) and Zn (II) Girard's T hydrazone complexes in solution and solid state: effect of H-bonding on coordination number and supramolecular assembly of Cd(II) complex in solid state, Struct. Chem. (2018) 1–10, https://doi.org/10.1007/s11224-018-1155-8.

[108] T.R. Todorović, A. Bacchi, N.O. Juranić, D.M. Sladić, G. Pelizzi, T.T. Božić, N.R. Filipović, K.K. Anđelković, Synthesis and characterization of novel Cd(II), Zn (II) and Ni(II) complexes with 2-quinolinecarboxaldehyde selenosemicarbazone. Crystal structure of bis(2-quinolinecarboxaldehyde selenosemicarbazonato)nickel (II), Polyhedron 26 (2007) 3428–3436, https://doi.org/10.1016/j.poly.2007.03.023.

[109] R.A. Allred, S.A. Huefner, K. Rudzka, A.M. Arif, L.M. Berreau, A cadmium hydroxide complex of a N_3 S-donor ligand containing two hydrogen bond donors: synthesis, characterization, and CO_2 reactivity, Dalton Trans. (2007) 351–357, https://doi.org/10.1039/B612748G.

[110] P. Saxena, N. Thirupathi, Reactions of $Cd(OAc)_2{\cdot}2H_2O$ with variously substituted pyridines. Efforts to unravel the factors that determine structure/nuclearity of the products, Polyhedron 98 (2015) 238–250, https://doi.org/10.1016/J.POLY.2015.06.002.

[111] G.R. Fulmer, A.J.M. Miller, N.H. Sherden, H.E. Gottlieb, A. Nudelman, B.M. Stoltz, J.E. Bercaw, K.I. Goldberg, NMR chemical shifts of trace impurities: common laboratory solvents, organics, and gases in deuterated solvents relevant to the organometallic chemist, Organometallics 29 (2010) 2176–2179, https://doi.org/10.1021/om100106e.

[112] M. Borsari, Cadmium: coordination chemistry, Encycl. Inorg. Bioinorg. Chem, John Wiley & Sons, Ltd, Chichester, UK, 2014, pp. 1–16, , https://doi.org/10.1002/9781119951438.eibc2261.

[113] F. Rubino, F. Maria Rubino, Toxicity of glutathione-binding metals: a review of targets and mechanisms, Toxics 3 (2015) 20–62, https://doi.org/10.3390/toxics3010020.

[114] M. Calligaris, O. Carugo, Structure and bonding in metal sulfoxide complexes, Coord. Chem. Rev. 153 (1996) 83–154, https://doi.org/10.1016/0010-8545(95)01193-5.

[115] T. Diao, P. White, I. Guzei, S.S. Stahl, Characterization of DMSO coordination to palladium(II) in solution and insights into the aerobic oxidation catalyst, Pd $(DMSO)_2$ $(TFA)_2$, Inorg. Chem. 51 (2012) 11898–11909, https://doi.org/10.1021/ic301799p.

[116] N.R. Filipović, S. Bjelogrlić, A. Marinković, T. Verbic, I.N. Cvijetić, M. Senćanski, M.V. Rodić, M. Vujčić, D. Sladić, Z. Striković, T.R. Todorović, C.D. Muller, Zn(II) complex with 2-quinolinecarboxaldehyde selenosemicarbazone: synthesis, structure, interaction studies with DNA/HSA, molecular docking and caspase-8 and -9 independent apoptose induction, RSC Adv. (2015) 95191–95211, https://doi.org/10.1039/C5RA19849F.

[117] A. Božić, A. Marinković, S. Bjelogrlić, T.R. Todorović, I.N. Cvijetić, I. Novaković, C.D. Muller, N.R. Filipović, Quinoline based mono- and bis-(thio)carbohydrazones: synthesis, anticancer activity in 2D and 3D cancer and cancer stem cell models, RSC Adv. 6 (2016), https://doi.org/10.1039/c6ra23940d.

[118] N.R. Filipović, S. Bjelogrlić, G. Portalone, S. Pelliccia, R. Silvestri, O. Klisurić, M. Senćanski, D. Stanković, T.R. Todorović, C.D. Muller, Pro-apoptotic and pro-differentiation induction by 8-quinolinecarboxaldehyde selenosemicarbazone and its Co(III) complex in human cancer cell lines, Med. Chem. Commun. 7 (2016) 1604–1616, https://doi.org/10.1039/C6MD00199H.

[119] N.R. Filipović, S. Bjelogrlić, T.R. Todorović, V.A. Blagojević, C.D. Muller, A. Marinković, M. Vujčić, B. Janović, A.S. Malešević, N. Begović, M. Senćanski, D.M. Minić, Ni(II) complex with bishydrazone ligand: synthesis, characterization, DNA binding studies and pro-apoptotic and pro-differentiation induction in human cancerous cell lines, RSC Adv. 6 (2016) 108726–108740, https://doi.org/10.1039/c6ra24604d.

[120] R. Marullo, E. Werner, N. Degtyareva, B. Moore, G. Altavilla, S.S. Ramalingam, P.W. Doetsch, Cisplatin induces a mitochondrial-ROS response that contributes to cytotoxicity depending on mitochondrial redox status and bioenergetic functions, PLoS One 8 (2013) e81162, , https://doi.org/10.1371/journal.pone.0081162.

[121] A.-M. Florea, D. Büsselberg, Cisplatin as an anti-tumor drug: cellular mechanisms of activity, drug resistance and induced side effects, Cancers (Basel) 3 (2011) 1351–1371, https://doi.org/10.3390/cancers3011351.

[122] K. Woźniak, J. Błasiak, Recognition and repair of DNA-cisplatin adducts, Acta Biochim. Pol. 49 (2002) 583–596 (doi:024903583).

[123] J.M. Malinge, M.J. Giraud-Panis, M. Leng, Interstrand cross-links of cisplatin induce striking distortions in DNA, J. Inorg. Biochem. 77 (1999) 23–29, https://doi.org/10.1016/S0162-0134(99)00148-8.

[124] J.M. Wagner, L.M. Karnitz, Cisplatin-induced DNA damage activates replication checkpoint signaling components that differentially affect tumor cell survival, Mol. Pharmacol. 76 (2009) 208–214, https://doi.org/10.1124/mol.109.055178.

[125] E.A. Kohn, N.D. Ruth, M.K. Brown, M. Livingstone, A. Eastman, Abrogation of the S phase DNA damage checkpoint results in S phase progression or premature mitosis depending on the concentration of 7-hydroxystaurosporine and the kinetics of Cdc25C activation, J. Biol. Chem. 277 (2002) 26553–26564, https://doi.org/10.1074/jbc.M202040200.

[126] R.T. Bunch, A. Eastman, 7-Hydroxystaurosporine (UCN-01) causes redistribution of proliferating cell nuclear antigen and abrogates cisplatin-induced S-phase arrest in Chinese hamster ovary cells, Cell Growth Differ. 8 (1997) 779–788.

[127] S.I. Lee, M.K. Brown, A. Eastman, Comparison of the efficacy of 7-hydroxystaurosporine (UCN-01) and other staurosporine analogs to abrogate cisplatin-induced cell cycle arrest in human breast cancer cell lines, Biochem. Pharmacol. 58 (1999) 1713–1721, https://doi.org/10.1016/S0006-2952(99)00258-0.

[128] C.M. Sorenson, A. Eastman, Influence of *cis*-diamminedichloroplatinum(II) on DNA synthesis and cell cycle progression in excision repair proficient and deficient Chinese hamster ovary cells, Cancer Res. 48 (1988) 6703–6707.

[129] C. Demarcq, R.T. Bunch, D. Creswell, A. Eastman, The role of cell cycle progression in cisplatin-induced apoptosis in Chinese hamster ovary cells, Cell Growth Differ. 5 (1994) 983–993.

[130] L.D. Attardi, A. de Vries, T. Jacks, Activation of the p53-dependent G1 checkpoint

response in mouse embryo fibroblasts depends on the specific DNA damage inducer, Oncogene 23 (2004) 973–980, https://doi.org/10.1038/sj.onc.1207026.
[131] G. He, J. Kuang, A.R. Khokhar, Z.H. Siddik, The impact of S- and G2-checkpoint response on the fidelity of G1-arrest by cisplatin and its comparison to a non-cross-resistant platinum(IV) analog, Gynecol. Oncol. 122 (2011) 402–409, https://doi.org/10.1016/j.ygyno.2011.04.034.
[132] X. Lu, J. Errington, N.J. Curtin, J. Lunec, D.R. Newell, The impact of p53 status on cellular sensitivity to antifolate drugs, Clin. Cancer Res. 7 (2001) 2114–2123.
[133] E.L. Deer, J. González-Hernández, J.D. Coursen, J.E. Shea, J. Ngatia, C.L. Scaife, M.A. Firpo, S.J. Mulvihill, Phenotype and genotype of pancreatic cancer cell lines, Pancreas 39 (2010) 425–435, https://doi.org/10.1097/MPA.0b013e3181c15963.
[134] S.W.G. Tait, D.R. Green, Caspase-independent cell death: leaving the set without the final cut, Oncogene 27 (2008) 6452–6461, https://doi.org/10.1038/onc.2008.311.
[135] L.L. Fava, F.J. Bock, S. Geley, A. Villunger, Caspase-2 at a glance, J. Cell Sci. 125 (2012) 5911–5915, https://doi.org/10.1242/jcs.115105.
[136] R. Huang, A. Wallqvist, D.G. Covell, Anticancer metal compounds in NCI's tumor-screening database: putative mode of action, Biochem. Pharmacol. 69 (2005) 1009–1039, https://doi.org/10.1016/j.bcp.2005.01.001.
[137] J. Zhao, L. Zhang, J. Li, T. Wu, M. Wang, G. Xu, F. Zhang, L. Liu, J. Yang, S. Sun, A novel pyrazolone-based derivative induces apoptosis in human esophageal cells via reactive oxygen species (ROS) generation and caspase-dependent mitochondria-mediated pathway, Chem. Biol. Interact. 231 (2015) 1–9, https://doi.org/10.1016/j.cbi.2015.02.004.
[138] J. Wang, H. Zhu, X. Liu, Z. Liu, *N*-acetylcysteine protects against cadmium-induced oxidative stress in rat hepatocytes, J. Vet. Sci. 15 (2014) 485–493, https://doi.org/10.4142/jvs.2014.15.4.485.
[139] K. Sinha, P.B. Pal, P.C. Sil, Cadmium (Cd^{2+}) exposure differentially elicits both cell proliferation and cell death related responses in SK-RC-45, Toxicol. in Vitro 28 (2014) 307–318, https://doi.org/10.1016/j.tiv.2013.11.011.
[140] D.B. Zorov, M. Juhaszova, S.J. Sollott, Mitochondrial reactive oxygen species (ROS) and ROS-induced ROS release, Physiol. Rev. 94 (2014) 909–950, https://doi.org/10.1152/physrev.00026.2013.
[141] M.P. Murphy, How mitochondria produce reactive oxygen species, Biochem. J. 417 (2009) 1–13, https://doi.org/10.1042/BJ20081386.
[142] J.J. Cullen, C. Weydert, M.M. Hinkhouse, J. Ritchie, F.E. Domann, D. Spitz, L.W. Oberley, The role of manganese superoxide dismutase in the growth of pancreatic adenocarcinoma, Cancer Res. 63 (2003) 1297–1303.
[143] L. Papa, M. Hahn, E.L. Marsh, B.S. Evans, D. Germain, SOD2 to SOD1 switch in breast cancer, J. Biol. Chem. 289 (2014) 5412–5416, https://doi.org/10.1074/jbc.C113.526475.
[144] S. Andrzejewski, S.-P. Gravel, M. Pollak, J. St-Pierre, Metformin directly acts on mitochondria to alter cellular bioenergetics, Cancer Metab. 2 (2014) 1–14, https://doi.org/10.1186/2049-3002-2-12.
[145] L.A. Sena, N.S. Chandel, Physiological roles of mitochondrial reactive oxygen species, Mol. Cell 48 (2012) 158–167, https://doi.org/10.1016/j.molcel.2012.09.025.
[146] F. Weinberg, R. Hamanaka, W.W. Wheaton, S. Weinberg, J. Joseph, M. Lopez, B. Kalyanaraman, G.M. Mutlu, G.R.S. Budinger, N.S. Chandel, Mitochondrial metabolism and ROS generation are essential for Kras-mediated tumorigenicity, Proc. Natl. Acad. Sci. 107 (2010) 8788–8793, https://doi.org/10.1073/pnas.1003428107.
[147] G.W.A. Dummer, J.M. Robertson, Medical Electronic Laboratory Equipment, 1967–68, Elsevier Ltd, 2014.
[148] B. Galateanu, A. Hudita, C. Negrei, R.M. Ion, M. Costache, M. Stan, D. Nikitovic, A.W. Hayes, D.A. Spandidos, A.M. Tsatsakis, O. Ginghina, Impact of multicellular tumor spheroids as an in vivo-like tumor model on anticancer drug response, Int. J. Oncol. 48 (2016) 2295–2302, https://doi.org/10.3892/ijo.2016.3467.
[149] M. Ravi, V. Paramesh, S.R. Kaviya, E. Anuradha, F.D.P. Solomon, 3D cell culture systems: advantages and applications, J. Cell. Physiol. 230 (2015) 16–26, https://doi.org/10.1002/jcp.24683.
[150] H. Elshaflu, S. Bjelogrlić, C.D. Muller, T.R. Todorović, M. Rodić, A. Marinković, N.R. Filipović, Co(III) complex with (*E*)-2-(2-(pyridine-2-ylmethylene)hydrazinyl)-4-(4-tolyl)-1,3-thiazole: structure and activity against 2-D and 3-D cancer cell models, J. Coord. Chem. 69 (2016) 3354–3366, https://doi.org/10.1080/00958972.2016.1232404.
[151] Ö. Karaca, S.M. Meier-Menches, A. Casini, F.E. Kühn, On the binding modes of metal NHC complexes with DNA secondary structures: implications for therapy and imaging, Chem. Commun. 53 (2017) 8249–8260, https://doi.org/10.1039/C7CC03074F.
[152] M. Fojta, A. Daňhel, L. Havran, V. Vyskočil, Recent progress in electrochemical sensors and assays for DNA damage and repair, TrAC Trends Anal. Chem. 79 (2016) 160–167, https://doi.org/10.1016/j.trac.2015.11.018.
[153] M.J. Waring, Complex formation between ethidium bromide and nucleic acids, J. Mol. Biol. 13 (1965) 269–282, https://doi.org/10.1016/S0022-2836(65)80096-1.
[154] R. Kakkar, R. Garg, Suruchi, Towards understanding the molecular recognition process in Hoechst–DNA complexes, J. Mol. Struct. 584 (2002) 37–44, https://doi.org/10.1016/S0166-1280(02)00026-X.
[155] X. Ling, W. Zhong, Q. Huang, K. Ni, Spectroscopic studies on the interaction of pazufloxacin with calf thymus DNA, J. Photochem. Photobiol. B 93 (2008) 172–176, https://doi.org/10.1016/j.jphotobiol.2008.07.008.
[156] C. Icsel, V.T. Yilmaz, In vitro DNA binding studies of the sweetening agent saccharin and its copper(II) and zinc(II) complexes, J. Photochem. Photobiol. B 130 (2014) 115–121, https://doi.org/10.1016/J.JPHOTOBIOL.2013.11.001.
[157] A. Lagarto Parra, R. Silva Yhebra, I. Guerra Sardiñas, L. Iglesias Buela, Comparative study of the assay of *Artemia salina* L. and the estimate of the medium lethal dose (LD50 value) in mice, to determine oral acute toxicity of plant extracts, Phytomedicine 8 (2001) 395–400, https://doi.org/10.1078/0944-7113-00044.
[158] B. Birdsall, R.W. King, M.R. Wheeler, C.A. Lewis, S.R. Goode, R.B. Dunlap, G.C. Roberts, Correction for light absorption in fluorescence studies of protein-ligand interactions, Anal. Biochem. 132 (1983) 353–361.
[159] B. Ojha, G. Das, The interaction of 5-(Alkoxy)naphthalen-1-amine with bovine serum albumin and its effect on the conformation of protein, J. Phys. Chem. B 114 (2010) 3979–3986, https://doi.org/10.1021/jp907576r.
[160] J.R. Lakowicz, Principles of Fluorescence Spectroscopy, 3rd ed., Springer Science Business Media, New York, USA, 2006.